Electronic Supplementary Material (ESI) for Journal of Materials Chemistry C.

Electronic Supplementary Information

Fast Photo Stimulus Responsive Ultralong Room-temperature Phosphorescence Behaviour of Benzoic Acid Derivatives @ Boric acid

Yi Cheng, Wenwen Fan, Longjie Wang, Yanxiong Liu, Shaoxiong Yang, Yonggang Shi, Shixi Liu,* Liyan Zheng,* Qiue Cao*

Table of Contents

1. Experimental section

1.1 Chemicals and materials

All benzoic acid derivatives, boric acid and PMMA were purchased from Energy Chemical and without further purification unless otherwise noted. Dichloromethane and absolute ethanol were purchased from General-Reagent. Doubly distilled water was used throughout the experiments and was prepared using a Milli-Q water purification system.

1.2 Synthesis of BADs@BA and BADs@PMMA

Synthesis of four kinds of BADs@BA at different doped ratio: 3 g (48.5 mmol) BA were firstly diluted with 40 mL doubly distilled water in a beaker and mixed with different molar BADs: 0.97 mmol, 0.485 mmol, 0.2425 mmol, 97 μmol, 48.5 μmol, 24.25 μmol, 12.125 μmol, 6.0625 μmol ($n_{BADs} : n_{BA} = 1 : 50, 1 : 100, 1 : 200, 1 : 500, 1 : 1000, 1 : 2000, 1 : 4000, 1 : 8000$), respectively. Then the beaker was covered with foil to prevent the water from evaporating too fast. And the beaker was put in an oven at 180 ℃ for 5 h and cooled down to room temperature naturally. The final glassy state BADs@BA were ground into powder by ball milling.

Synthesis of IPA@BA at different temperature: 3 g (48.5 mmol) BA were firstly diluted with 40 mL doubly distilled water in a beaker and mixed with the best molar ratio IPA. Then the beaker was covered with foil to prevent the water from evaporating too fast. And the beaker was put in an oven at different temperature (100 ℃, 120 ℃, 140 ℃, 160 ℃ and 180 ℃, respectively) for 5 h and cooled down to room temperature naturally.

Synthesis of four kinds of BADs@PMMA at different doped ratio: 3 g PMMA were firstly diluted with 80 mL dichloromethane in a beaker. BADs were dissolved in ethanol with different molar: 0.485 mmol, 0.2425 mmol, 97 μmol, 48.5 μmol, 24.25 μmol, 12.125 μmol and 6.0625 μmol,

respectively. Then mixed them and slowly evaporated under 40 ℃ in a day, the solid BADs@PMMA were obtained.

1.3 The quantitative method for PA

A collection system for sublimated PA was built as shown in Fig. S7. NaOH solution (0.1 mol, 200 mL) was used to collect the sublimated PA and used acid-base titration to determine the last NaOH concentration. Finally, the amount of sublimated PA was calculated by the NaOH concentration.

1.4 Characterizations

Powder X-ray diffraction (RXRD) was performed by using a YYRIII X-30 ray diffractometer (Rigaku, Japan) with CuKa radiation at 40 kV and 200 mA. Fourier transform-infrared spectroscopy (FT-IR) spectra were recorded in the range 4000-400 cm^{-1} using a Thermo Nicolet spectrometer with KBr pellets. Ground-state stimulated Raman spectra were recorded in the range 1500-150 cm^{-1} using HR evolution (Horiba Jobin Yvon, Japan) with 785 nm laser excitation. Photoluminescence spectra and afterglow decay curves were recorded with Horiba Jobin Yvon Fluorolog-3. Thermogravimetric analysis (TGA) was performed by using a NETZSCH STA 449F3 instrument with a heating rate of 10 °C min^{-1} under a nitrogen atmosphere. UV-Vis spectroscopy was performed with a UV-2700 UV-Vis spectrophotometer (Shimadzu, Japan). XPS was performed using a K-Alpha X-ray photoelectron spectrometer. Temperature-dependent PL emission spectra, afterglow emission spectra, and afterglow decay curves were conducted by combining a heating apparatus (Oxford Instruments) with the same Horiba Jobin Yvon Fluorolog-3. ^{1}H NMR, ^{13}C NMR spectra were recorded on AVANCE DRX 400 spectrometer (Bruker,

German). Confocal laser scanning microscope (CLSM) images were performed with Leica TCS SP8 STED (Leica, German). The electron spin resonance (ESR) spectra were conducted by Bruker EMX Plus (Bruker, German). Electrospray ionization mass spectra were obtained with a High Performance 1100 Liquid Chromatography-Mass Spectrometer (Agilent Technologies, USA). Digital images and video were taken with Redmi K20 pro smartphone.

The phosphorescence measurement methods were based on time-dependent deep UV LED lighting system (275 nm). This system could set irradiation times and be used with CCD detector. The lighting system would be turned off when the set irradiation time was reached, and the CCD detector would start to detect the phosphorescence spectrum after 100 ms.

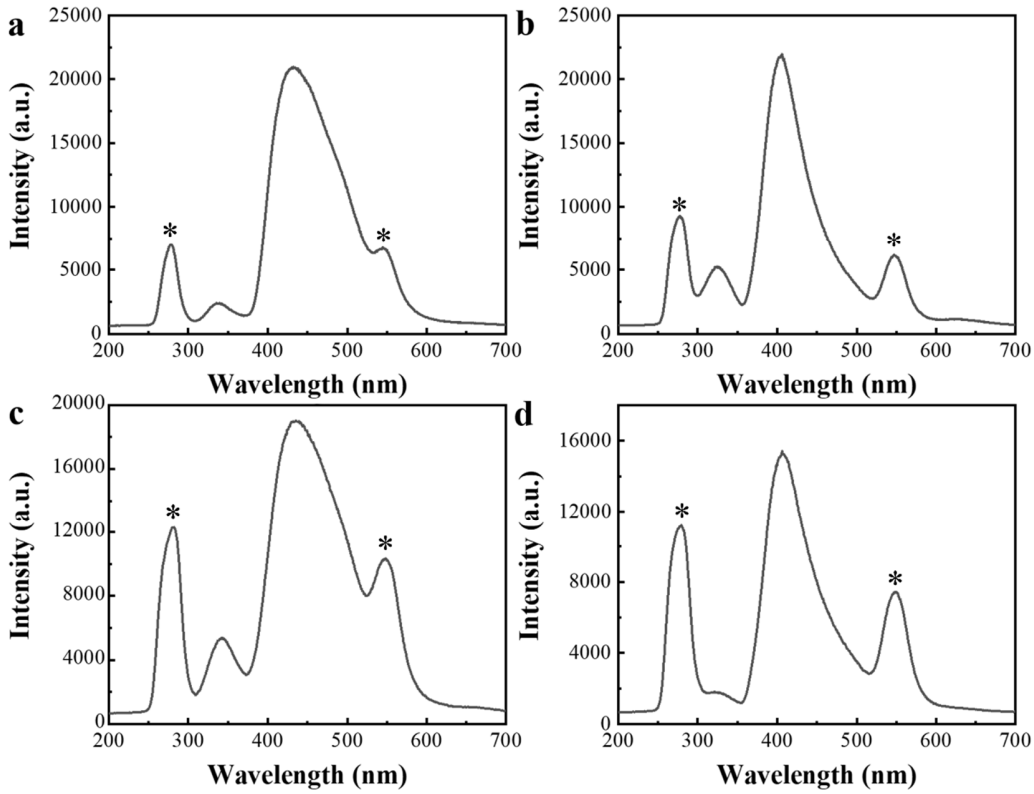

Fig. S1. (a) The lamp and PA@BA fluorescence emission spectrum. (b) The lamp and IPA@BA fluorescence emission spectrum. (c) The lamp and TPA@BA fluorescence emission spectrum. (d) The lamp and PA@BA fluorescence emission spectrum. (The lamp emission peaks were marked as asterisk.)

The period of photo-activation and deactivation of BADs@BA: Time-dependent phosphorescent spectra and time-dependent phosphorescent lifetimes were detected after 0.2 ~ 60 s UV irradiation; Kinetics spectra were used to detect the time-phosphorescent intensity and find the time that the phosphorescence completely disappeared. Reactivated time-dependent phosphorescent spectra were measured after 10, 15, 20, 30 and 60 s of switching off the UV light.

1.5 Theoretical calculations

CCDC 2127281 and CCDC 2127284 contains the supplementary crystallographic data for this paper. These data can be obtained free of charge from The Cambridge Crystallographic Data Centre via www.ccdc.cam.ac.uk/data_request/cif.

The computational model was built from the IPA crystal structures after 254 nm UV irradiation. The distribution of frontier molecule orbitals and excited states were obtained from the Gaussian09 program (version E.01).[1] The Becke's three-parameter exchange functional along with the M062X using 6-31G(d) basis sets were adopted throughout the calculation.[2]

For the microcrystal in BA matrix, a two-layer ONIOM model was adapted to perform hybrid QM/MM calculation.[3] The central QM part is described with quantum mechanics, whereas the surrounding MM part is treated using molecular force field (universal force field). The ground states and excited states geometries of the central QM part were optimized using M06-2X functional with 6-31G(d) basis set. The excitation energies of the n-th singlet excited states (S_n) and n-th triplet excited states (T_n) were calculated with TD-DFT method based on the optimized geometries. Intermolecular structure and stacking diagrams were drawn and measured by Olex2.[4] Nature transition orbits (NTOs) of S_1 and T_1 were analyzed by Multiwfn software package and VMD programs.[5, 6]

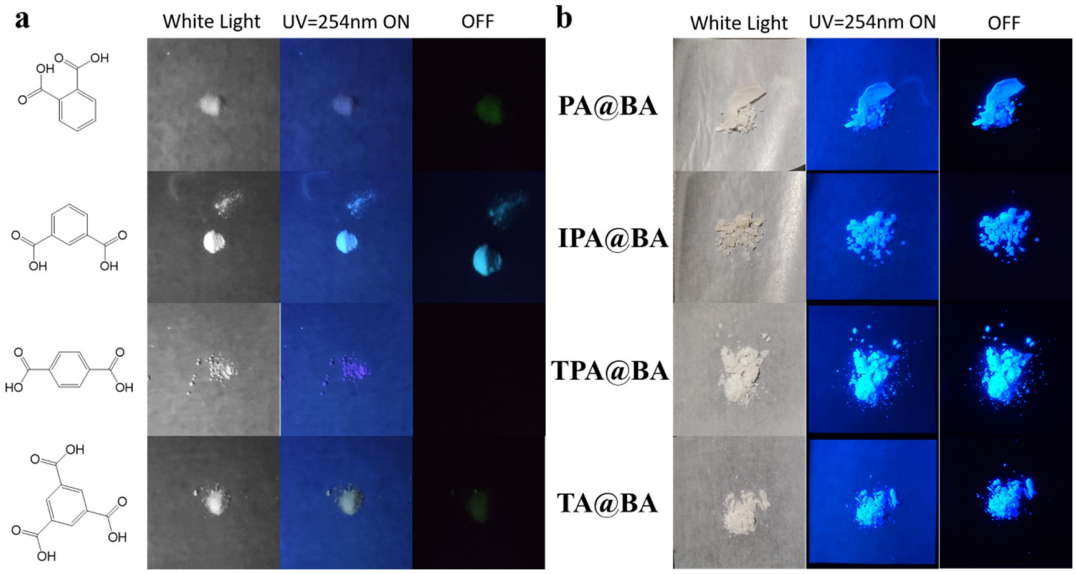

Fig. S2. (a) The fluorescence and phosphorescence photographs of phthalic acid (PA), isophthalic acid (IPA), terephthalic acid (TPA), and trimesic acid (TA) under 254 nm UV light. (b) The fluorescence and phosphorescence photographs of BADs@BA.

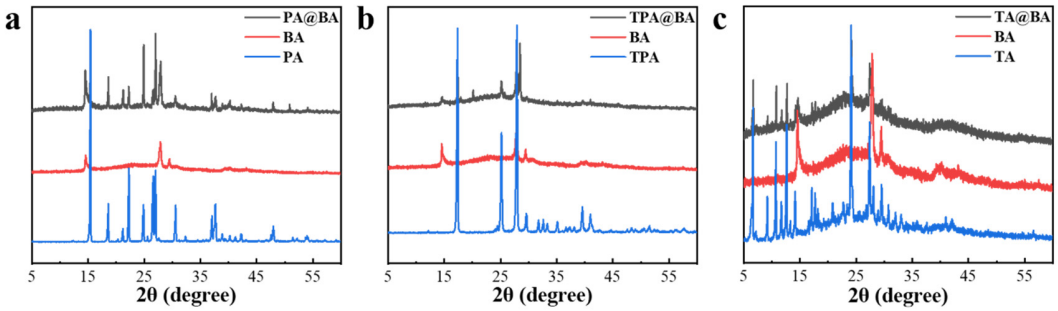

Fig. S3. (a) PXRD patterns of BA, PA, and PA@BA, respectively. (b) PXRD patterns of BA, TPA, and TPA@BA. (c) PXRD patterns of BA, TA, and TA@BA, respectively.

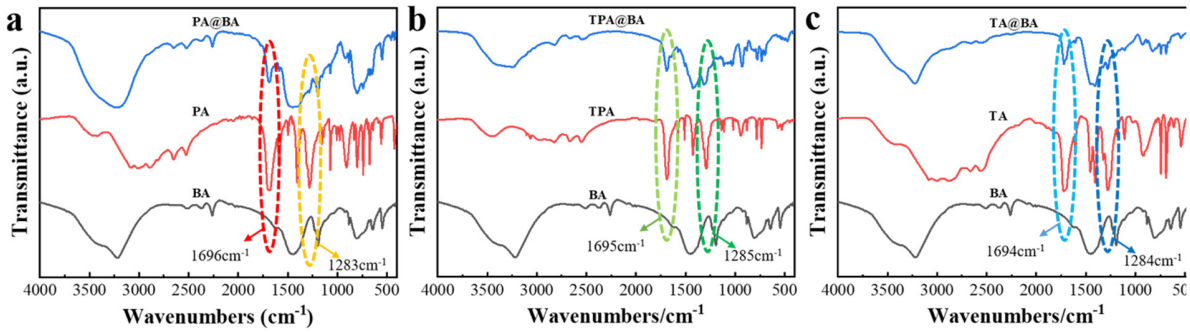

Fig. S4. (a) FT-IR spectra of BA, PA, and PA@BA, respectively. (b) FT-IR spectra of BA, TPA, and TPA@BA, respectively. (c) FT-IR spectra of BA, TA, and TA@BA, respectively.

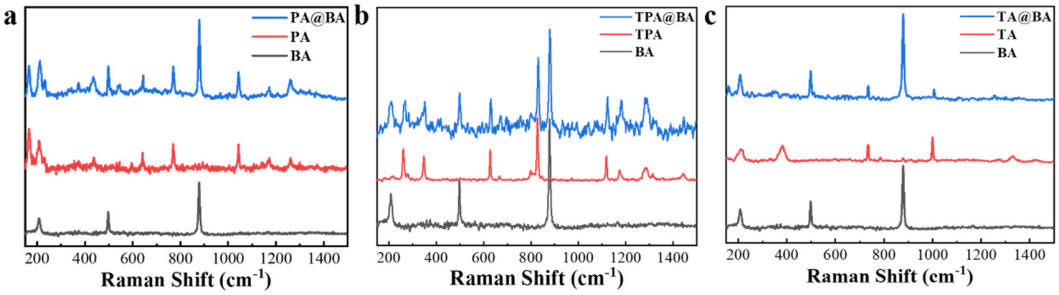

Fig. S5. (a) Raman spectra of BA, PA, and PA@BA, respectively. (b) Raman spectra of BA, TPA, and TPA@BA, respectively. (c) Raman spectra of BA, TA, and TA@BA, respectively.

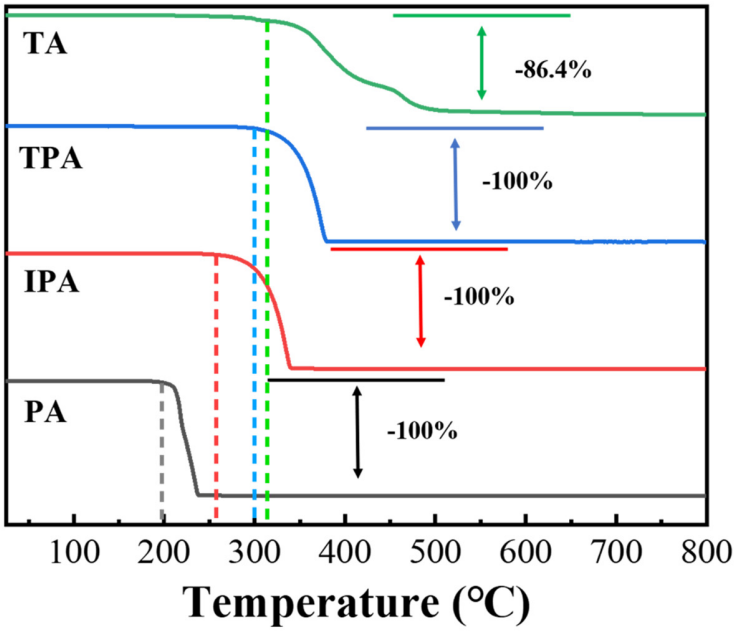

Fig. S6. Thermogravimetric analysis curves of PA, IPA, TPA and TA.

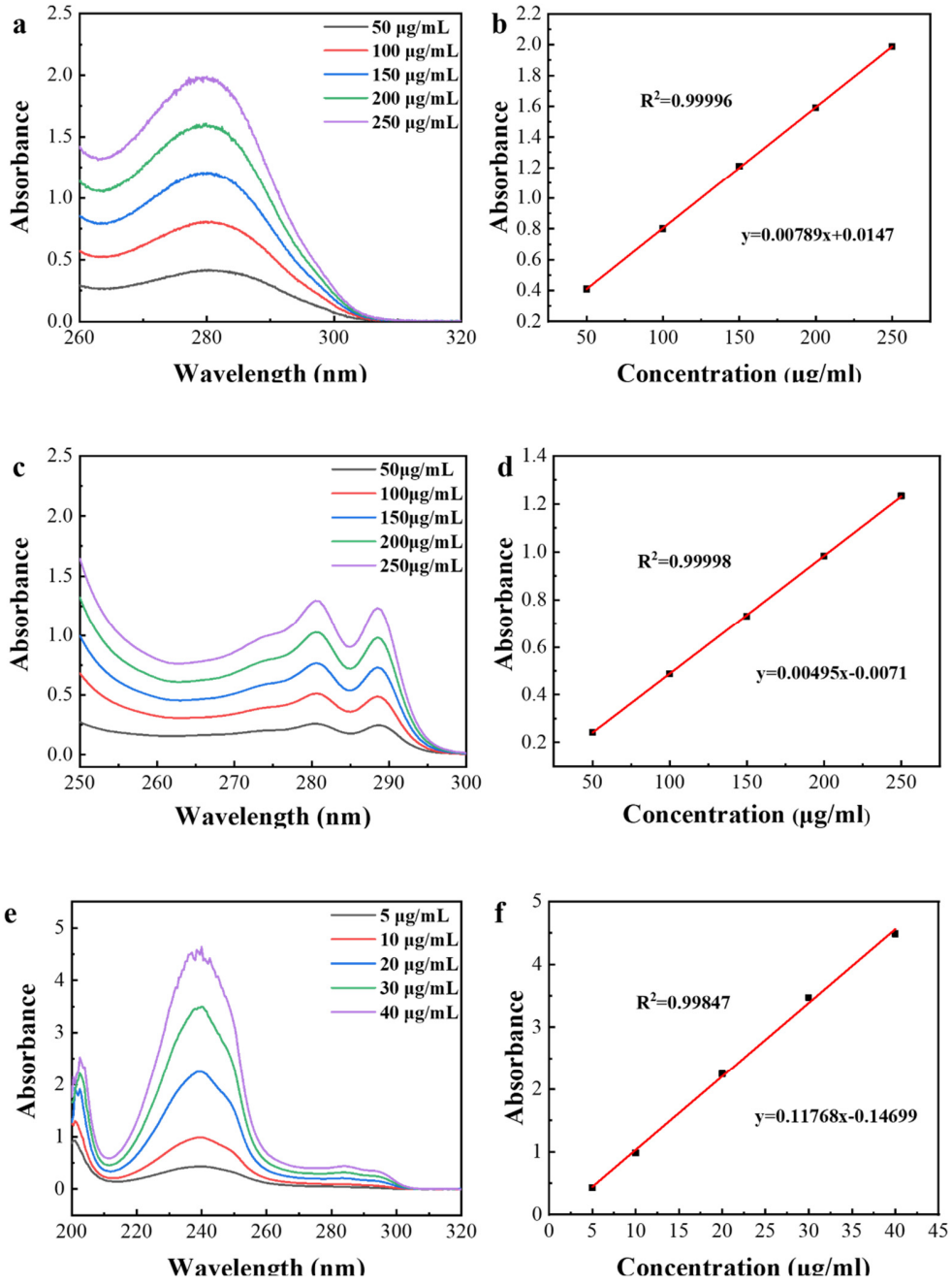
a
Absorbance
Wavelength (nm)
50 μg/mL
100 μg/mL
150 μg/mL
200 μg/mL
250 μg/mL
b
Absorbance
Concentration (μg/ml)
R²=0.99996
y=0.00789x+0.0147
c
Absorbance
Wavelength (nm)
50μg/mL
100μg/mL
150μg/mL
200μg/mL
250μg/mL
d
Absorbance
Concentration (μg/ml)
R²=0.99998
y=0.00495x-0.0071
e
Absorbance
Wavelength (nm)
5 μg/mL
10 μg/mL
20 μg/mL
30 μg/mL
40 μg/mL
f
Absorbance
Concentration (μg/ml)
R²=0.99847
y=0.11768x-0.14699

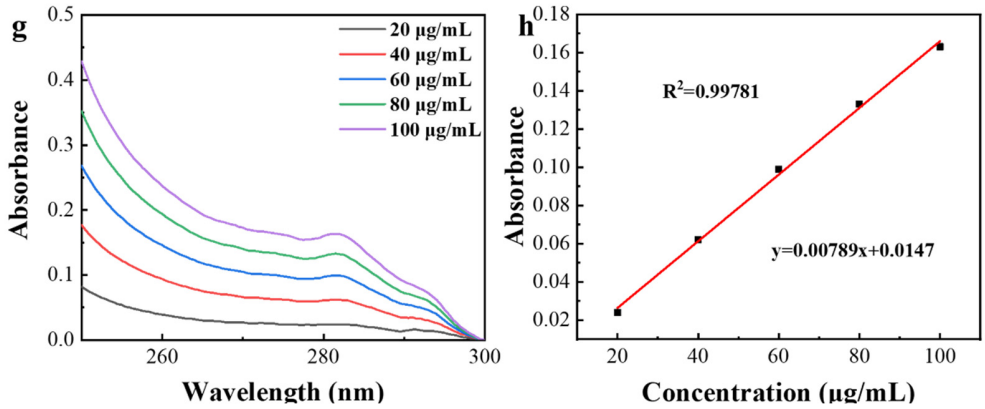

Fig. S7. (a) UV-Vis spectra of different concentration of PA solution. (b) The linear relationship between the concentration and UV-Vis absorbance of PA solution. (c) UV-Vis spectra of different concentration of IPA solution. (d) The linear relationship between the concentration and UV-Vis absorbance of IPA solution. (e) UV-Vis spectra of different concentration of TPA solution. (f) The linear relationship between the concentration and UV-Vis absorbance of TPA solution. (g) UV-Vis spectra of different concentration of TA solution. (h) The linear relationship between the concentration and UV-Vis absorbance of TA solution.

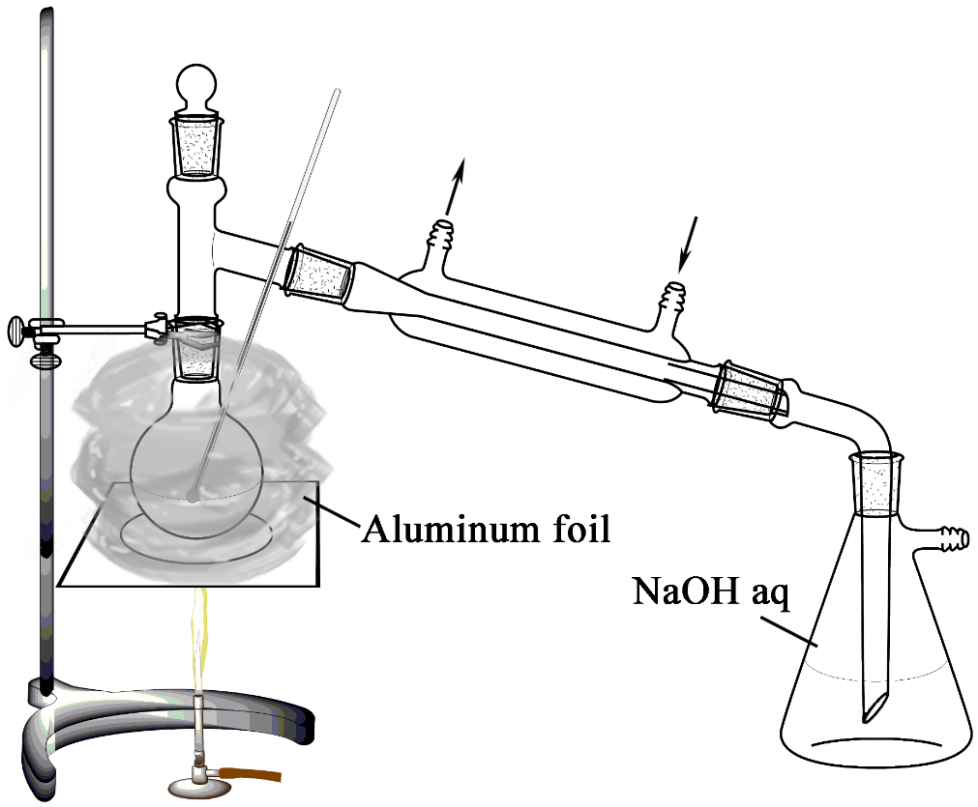

Fig. S8. The system to collect the sublimated PA.

Table S1. Quantitative determination of the benzoic acid derivatives' content in BADs@BA by UV-Vis spectra.

Samples	Absorbance	Average of absorbance	Theoretical content (mg)	Sublimation content (mg)	Actual content (mg)	Content percentage
	1.228					
PA@BA	1.055	1.192	76.809	2.874	80.000	99.604%
	1.293					
	0.674					
IPA@BA	0.759	0.725	80.999	-	80.000	101.249%
	0.743					
	2.302					
TPA@BA	2.587	2.475	79.348	-	80.000	99.184%
	2.537					
	0.032					
TA@BA	0.039	0.035	78.516	-	80.000	98.146%
	0.034					

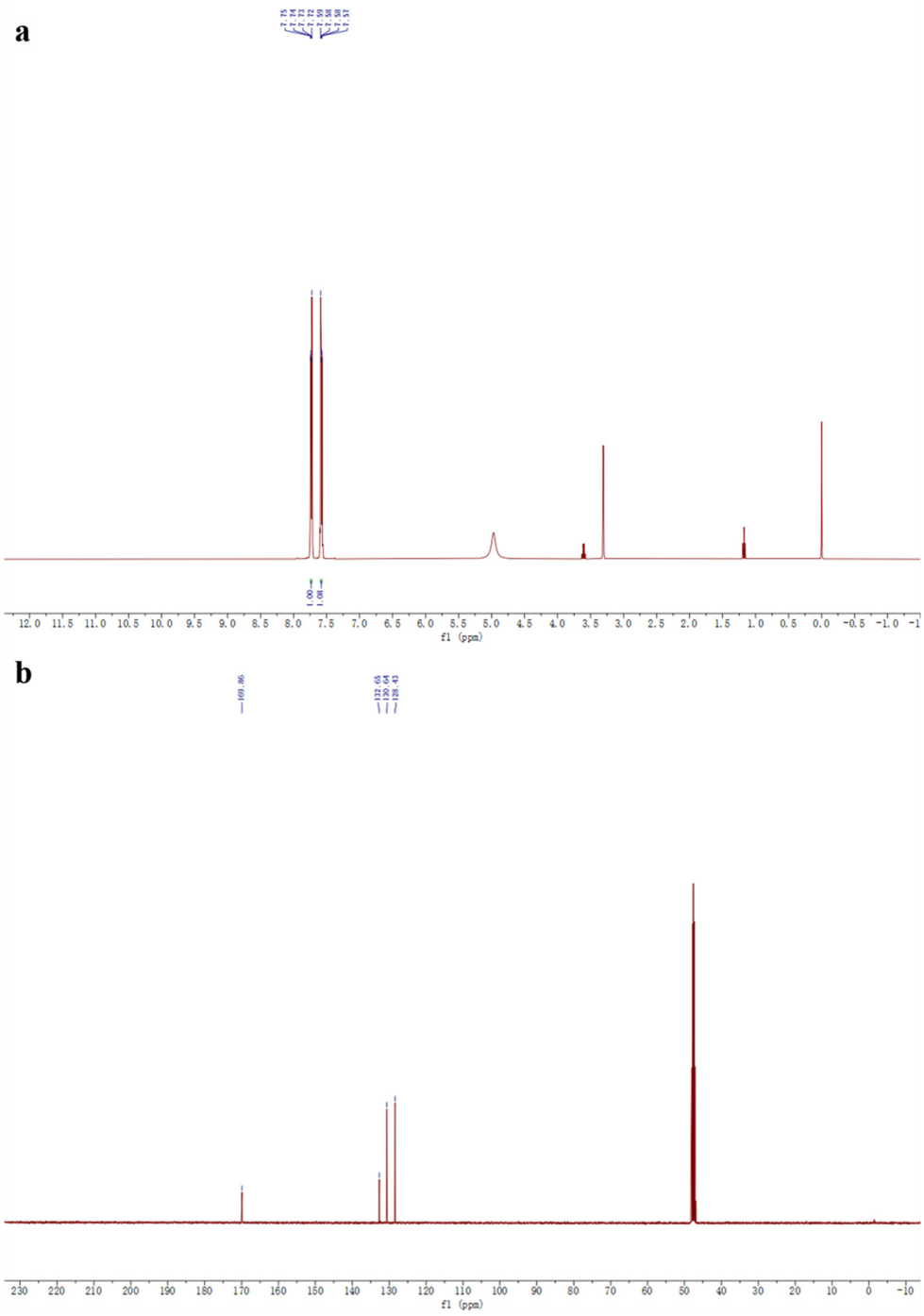

Fig. S9. (a) ^{1}H NMR spectrum of the PA@BA sublimation: ^{1}H NMR (400 MHz, D_2O) δ 7.73 (dd, J=4, 8 Hz, 2H), 7.58 (dd, J=4, 8 Hz, 2H). (b) ^{13}C NMR spectrum of the PA@BA sublimation: ^{13}C NMR (400 MHz, D_2O) δ 169.86, 132.65, 130.64, 128.43.

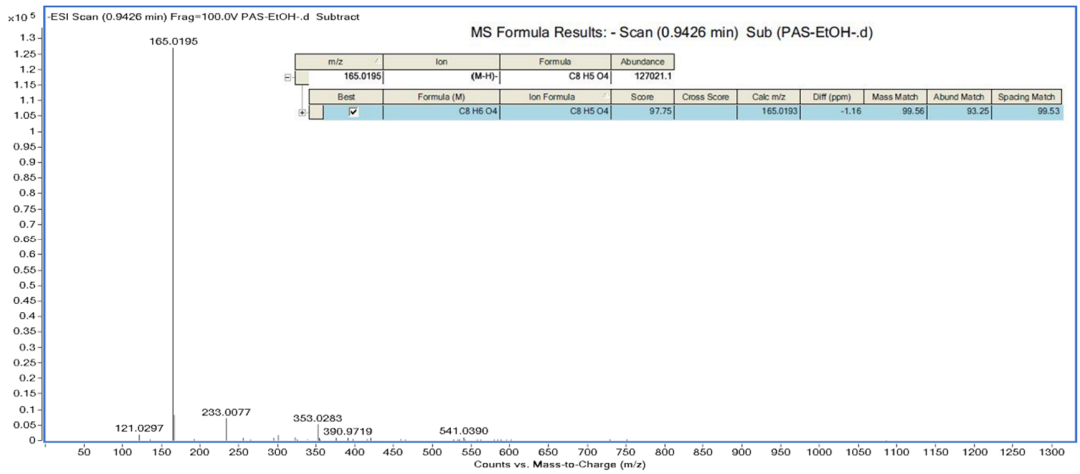

Fig. S10. Mass spectrum of the PA@BA sublimation

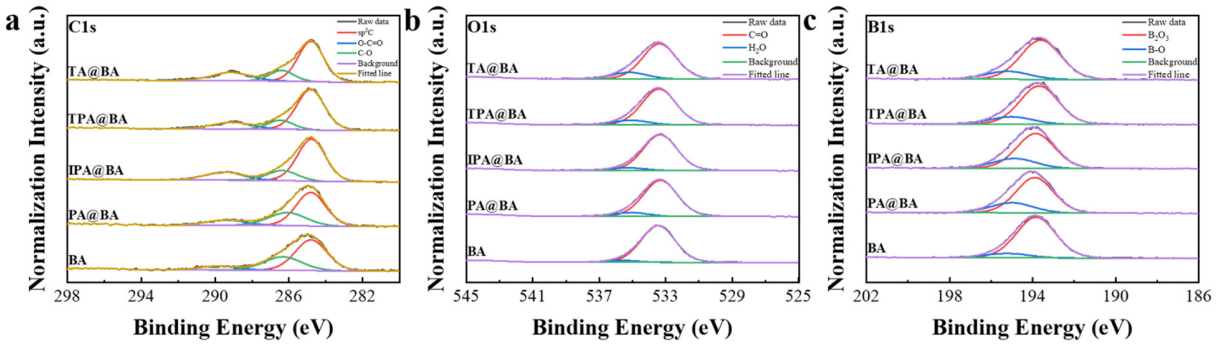

Fig. S11. (a) XPS high-resolution C1s spectra of BA, PA@BA, IPA@BA, TPA@BA and TA@BA, respectively. (b) XPS high-resolution O1s spectra of BA, PA@BA, IPA@BA, TPA@BA and TA@BA, respectively. (c) XPS high-resolution B1s spectra of BA, PA@BA, IPA@BA, TPA@BA and TA@BA, respectively.

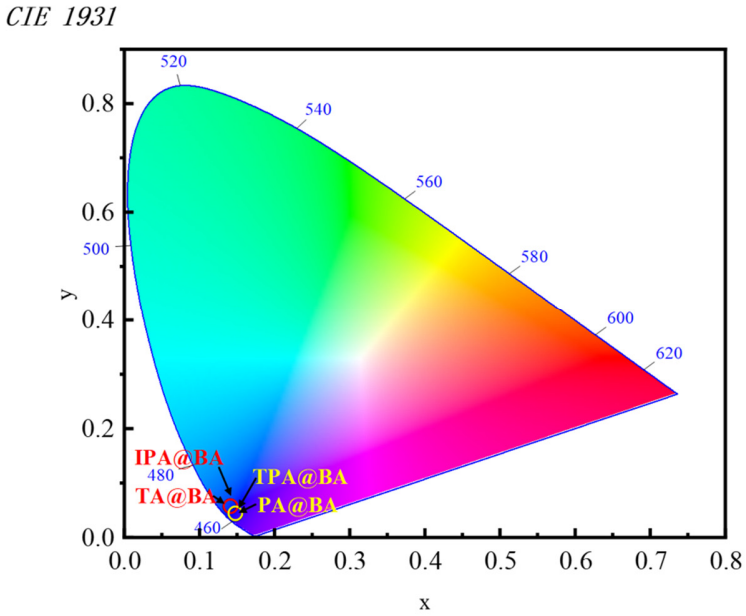

Fig. S12 . CIE coordinates of BADs@BA. PA@BA: (0.148, 0.044); IPA@BA: (0.141, 0.057); TPA@BA: (0.148, 0.044); TA@BA: (0.141, 0.057).

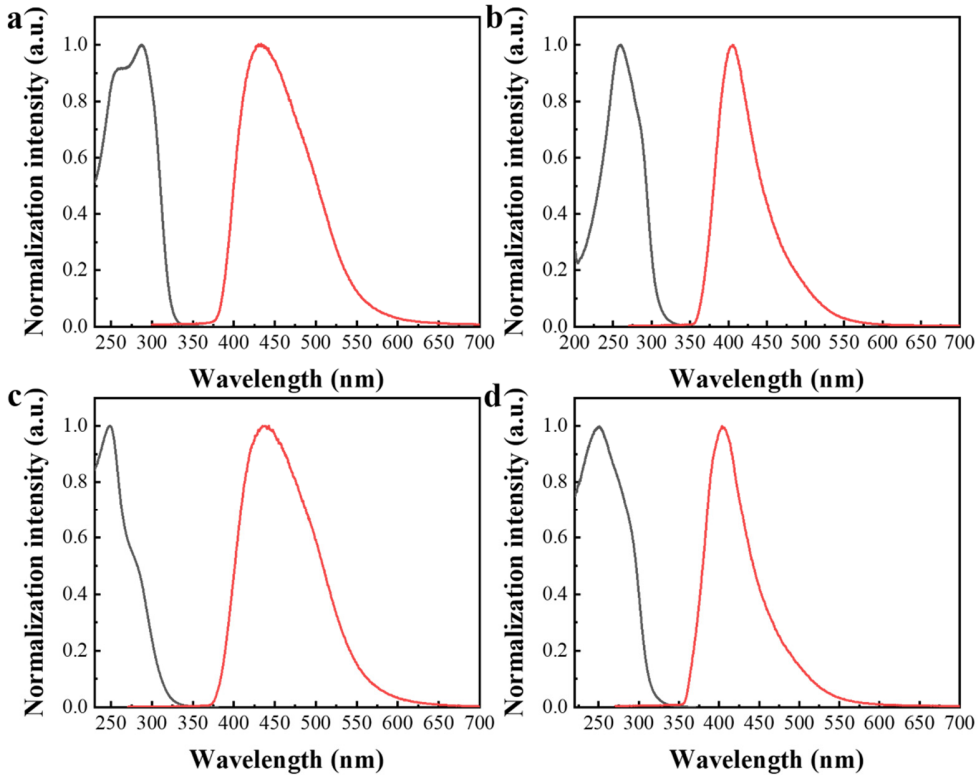

Fig. S13. (a) The phosphorescence excitation (black) and emission (red) spectra of PA@BA. (b) The phosphorescence excitation (black) and emission (red) spectra of IPA@BA. (c) The

phosphorescence excitation (black) and emission (red) spectra of TPA@BA. (d) The phosphorescence excitation (black) and emission (red) of TA@BA.

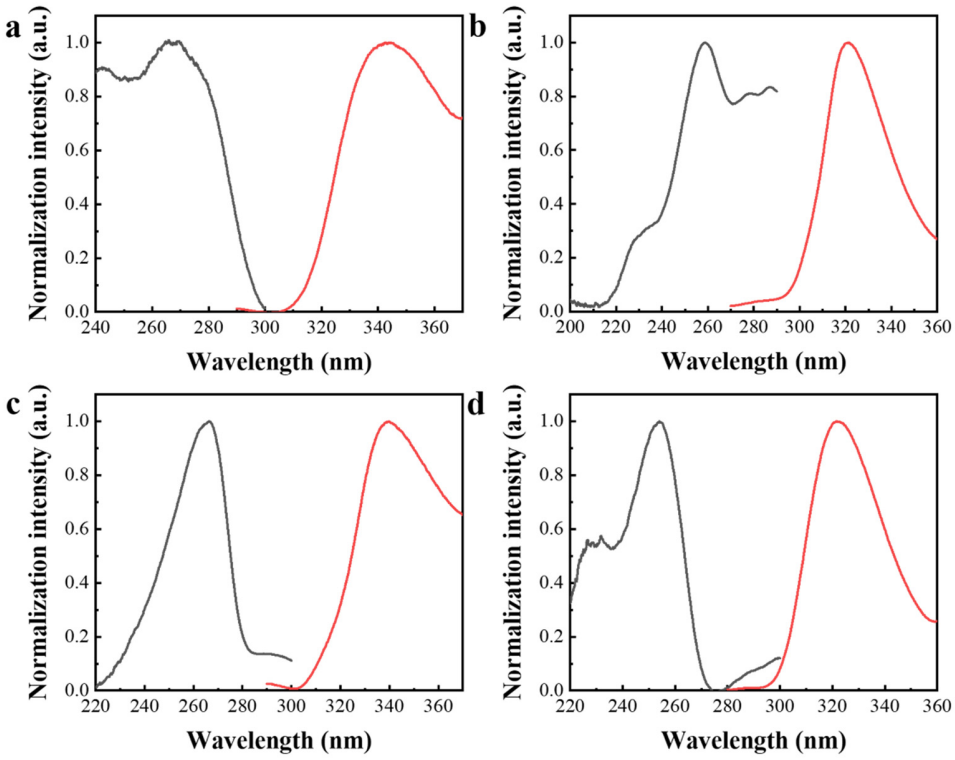

Fig. S14. (a) The excitation and emission fluorescence spectra of PA@BA. (b) The excitation and emission fluorescence spectra of IPA@BA. (c) The excitation and emission fluorescence spectra of TPA@BA. (d) The excitation and emission fluorescence spectra of TA@BA.

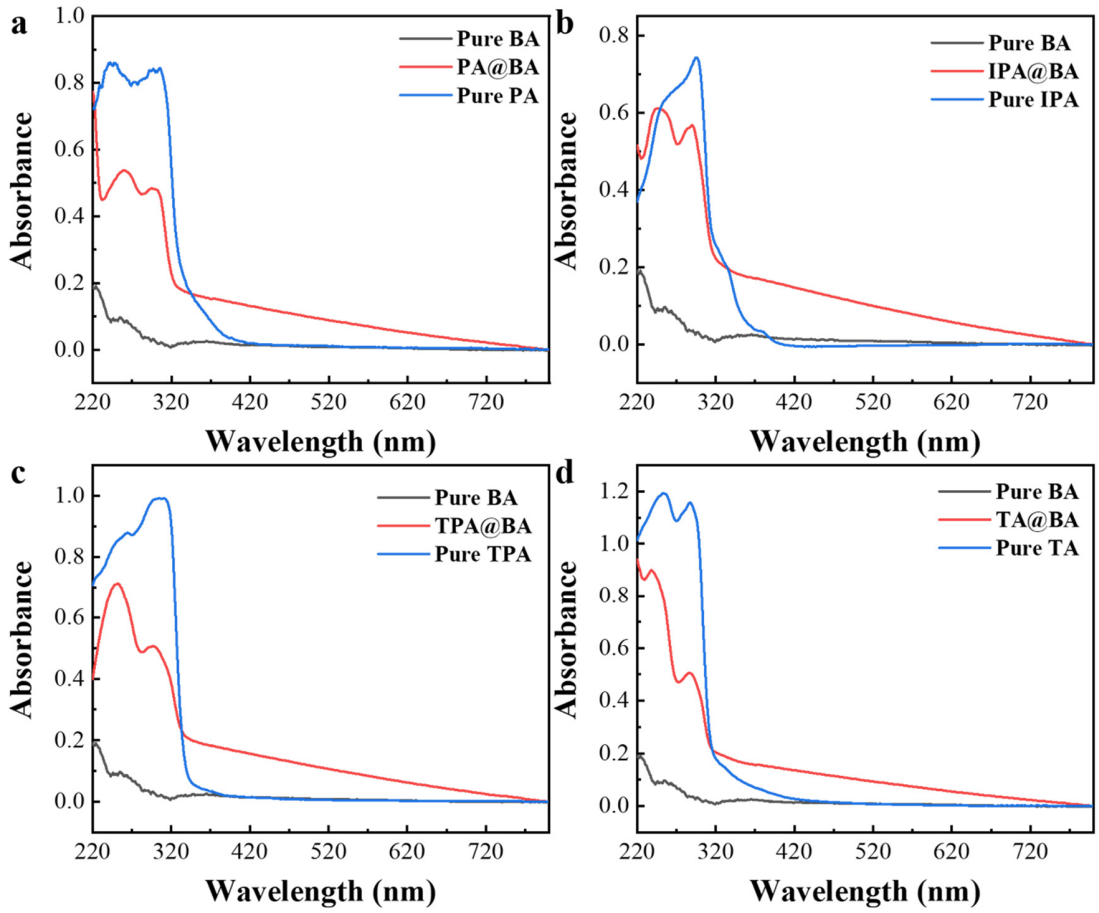

Fig. S15. (a) The solid-state UV-Vis spectra of PA, PA@BADs and pure BA. (b) The solid-state UV-Vis spectra of IPA, IPA@BADs and pure BA. (c) The solid-state UV-Vis spectra of TPA, TPA@BADs and pure BA. (d) The solid-state UV-Vis spectra of TA, TA@BADs and pure BA.

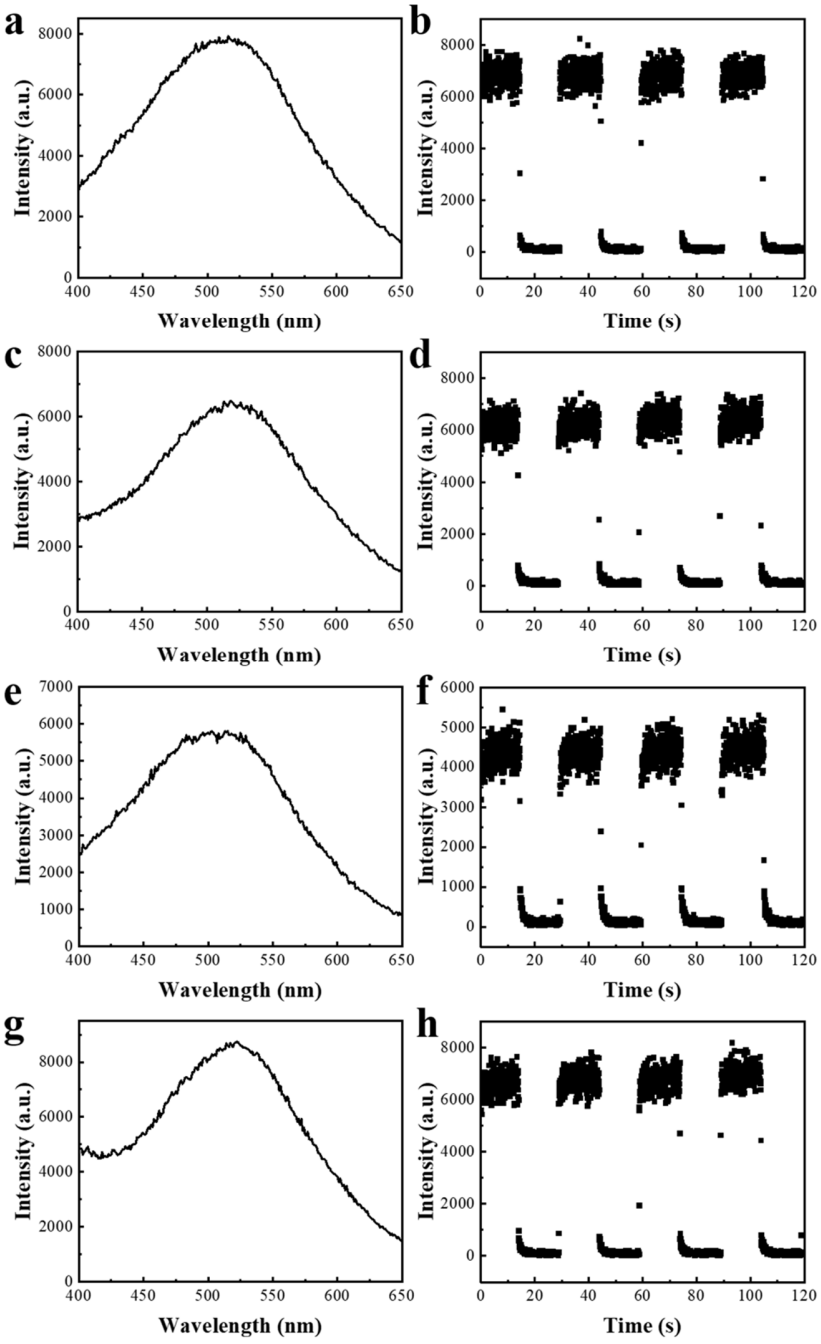

Fig. S16. (a), (b) The PA@BA phosphorescence spectrum and the cycles by on/off the shutter (λ_{em}=520 nm) under the λ_{ex}=365 nm, 298 K. (c), (d) The IPA@BA phosphorescence spectrum and the cycles by on/off the shutter (λ_{em}=520 nm) under the λ_{ex}=365 nm, 298 K. (e), (f) The TPA@BA phosphorescence spectrum and the cycles by on/off the shutter (λ_{em}=520 nm) under the λ_{ex}=365 nm,

298 K. (g), (h) The TA@BA phosphorescence spectrum and the cycle sby on/off the shutter (λ_{em}=520 nm) under the λ_{ex}=365 nm, 298 K.

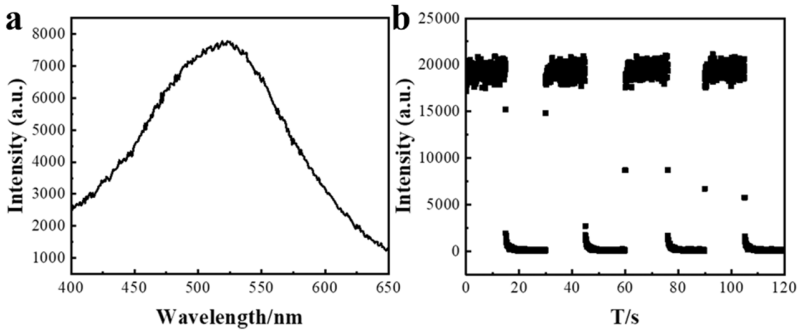

Fig. S17. (a), (b) The pure BA phosphorescence spectrum and the cycles by on/off the shutter (λ_{em}=520 nm) under the λ_{ex}=365 nm, 298 K;

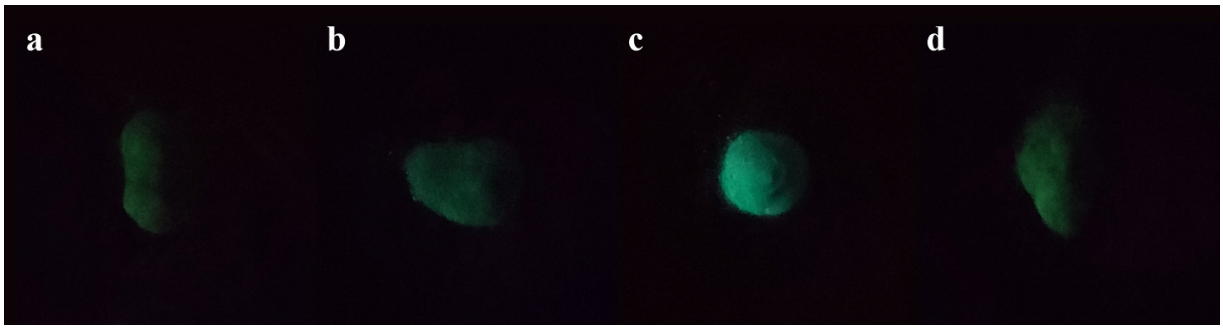

Fig. S18. (a) The phosphorescence image of PA@BA after irradiation by λ_{ex}=365 nm. (b) The phosphorescence image of IPA@BA after irradiation by λ_{ex}=365 nm. (c) The phosphorescence image of TPA@BA after irradiation by λ_{ex}=365 nm. (d) The phosphorescence image of TA@BA after irradiation by λ_{ex}=365 nm.

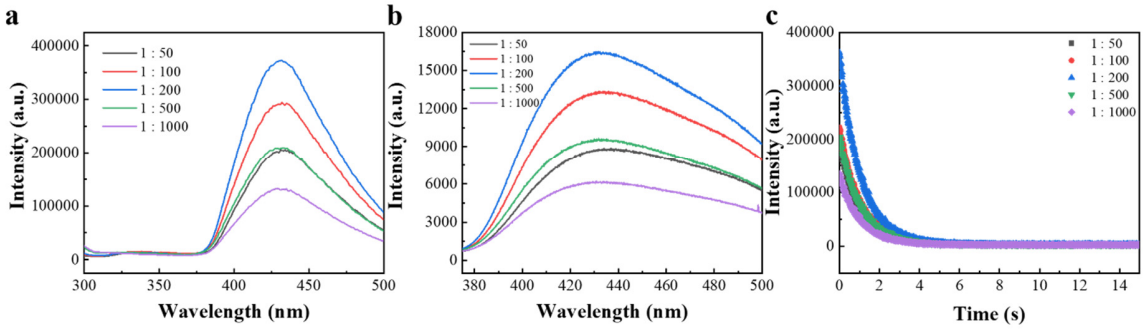

Fig. S19. (a), (b) and (c) fluorescence, phosphorescence spectra and lifetime decay profiles of different ratio PA@BA under ambient conditions.

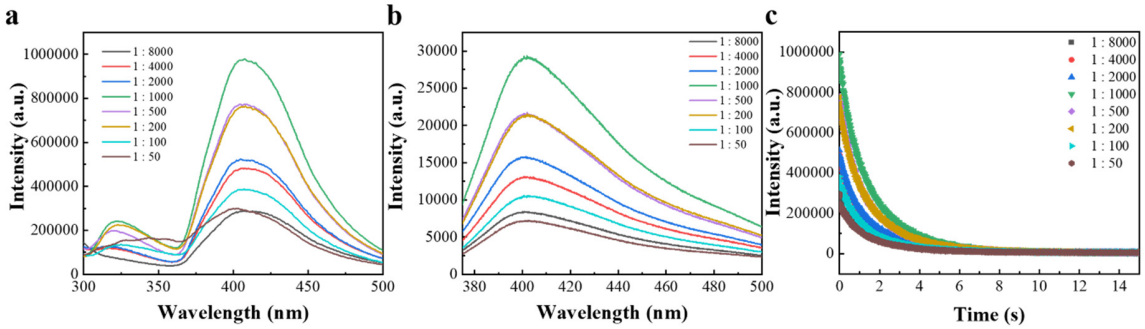

Fig. S20. (a), (b) and (c) fluorescence, phosphorescence spectra and lifetime decay profiles of different ratio IPA@BA under ambient conditions.

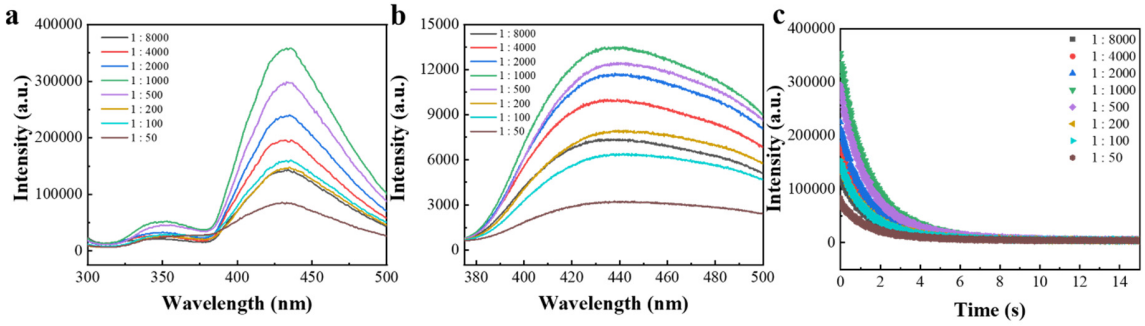

Fig. S21. (a), (b) and (c) fluorescence, phosphorescence spectra and lifetime decay profiles of different ratio TPA@BA under ambient conditions.

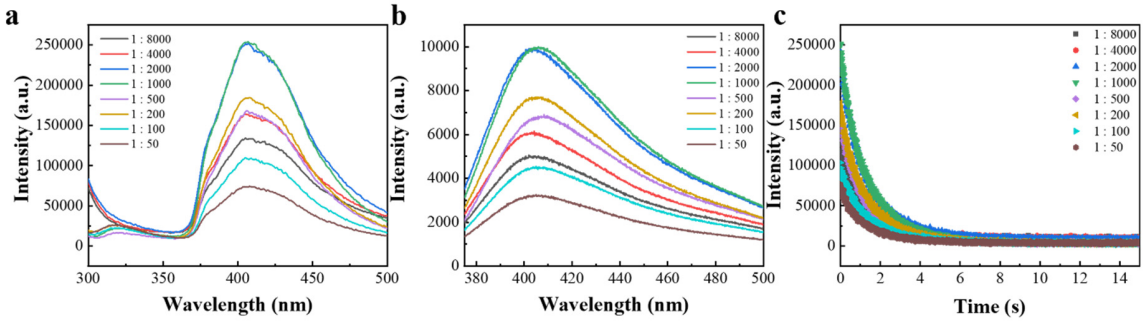

Fig. S22. (a), (b) and (c) fluorescence, phosphorescence spectra and lifetime decay profiles of different ratio TA@BA under ambient conditions.

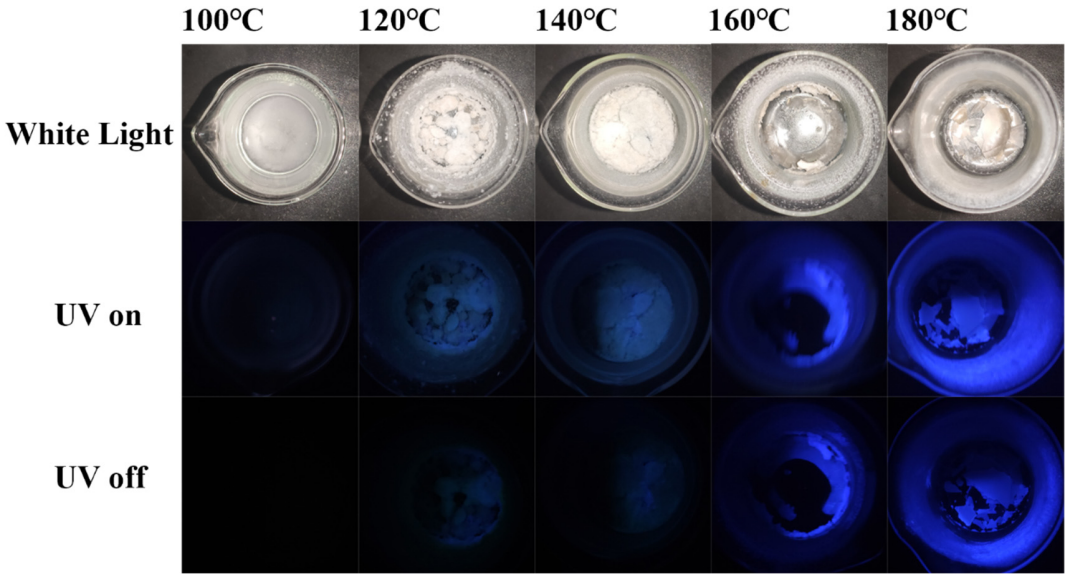

Fig. S23. The different synthesized temperature of IPA@BA under white light and 254 nm handy UV lamp.

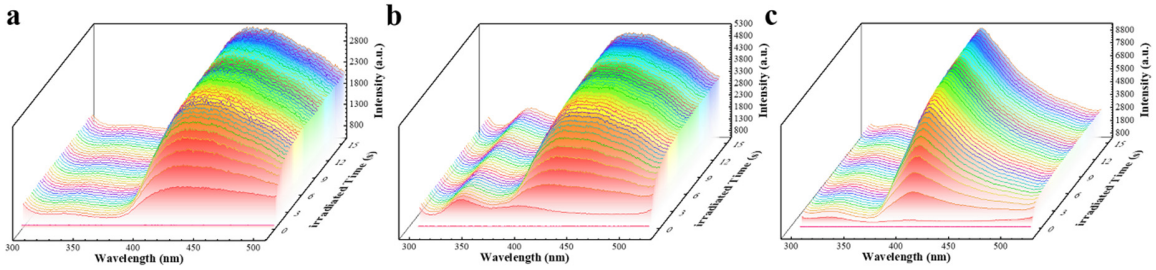

Fig. S24. (a) Fluorescence spectra of PA@BA excited at different seconds. (b) Fluorescence spectra of TPA@BA excited at different seconds. (c) Fluorescence spectra of TA@BA excited at different seconds.

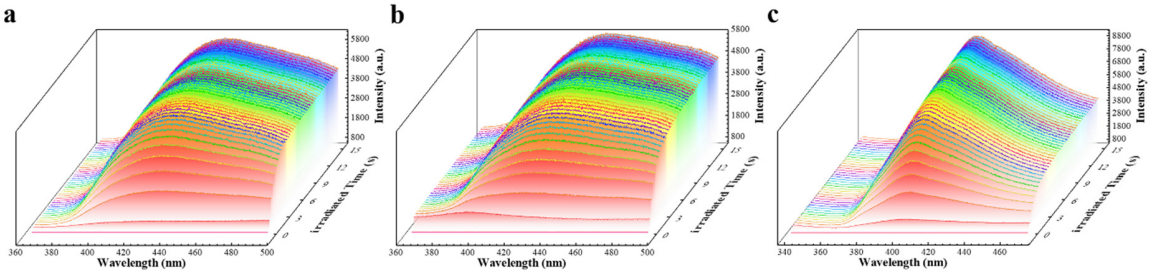

Fig. S25. (a) Phosphorescence spectra of PA@BA excited at different seconds. (b) Phosphorescence spectra of TPA@BA excited at different seconds. (c) Phosphorescence spectra of TA@BA excited at different seconds.

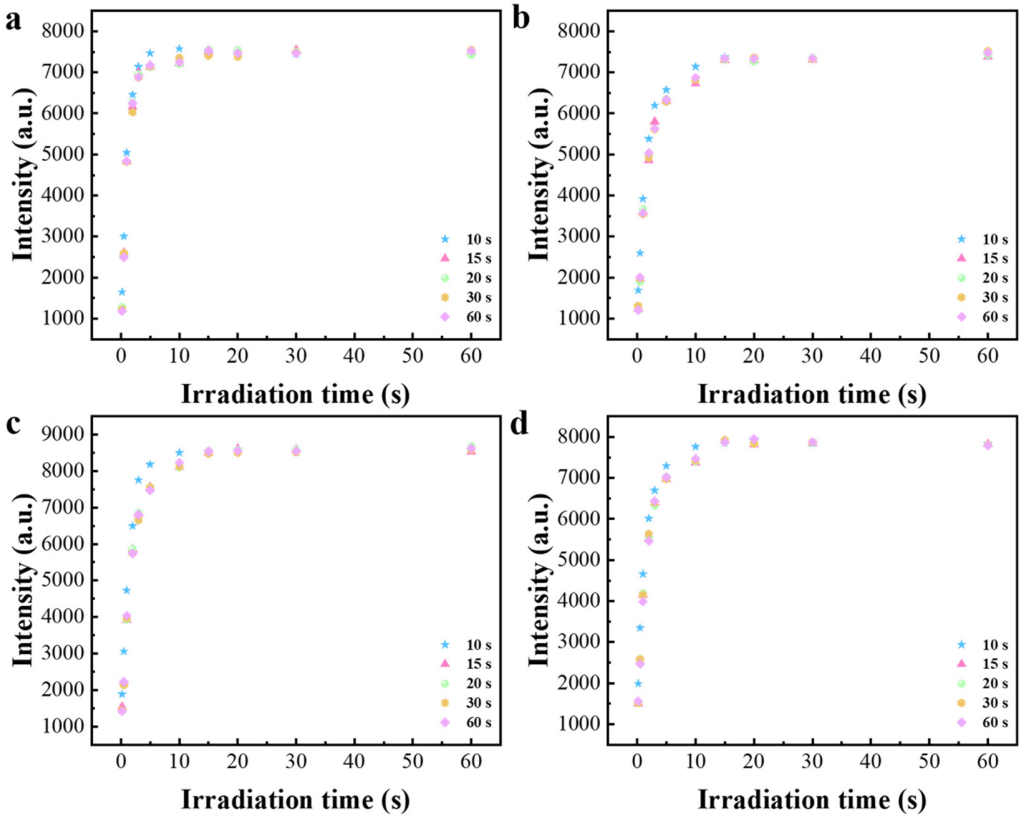

Fig. S26. (a) The photo-activation phosphorescent intensities of PA@BA after switching off 10, 15, 20, 30 and 60 s irradiation. (b) The photo-activation phosphorescent intensities of IPA@BA after switching off 10, 15, 20, 30 and 60 s irradiation. (c) The photo-activation phosphorescent intensities of TPA@BA after switching off 10, 15, 20, 30 and 60 s irradiation. (d) The photo-activation phosphorescent intensities of TA@BA after switching off 10, 15, 20, 30 and 60 s irradiation.

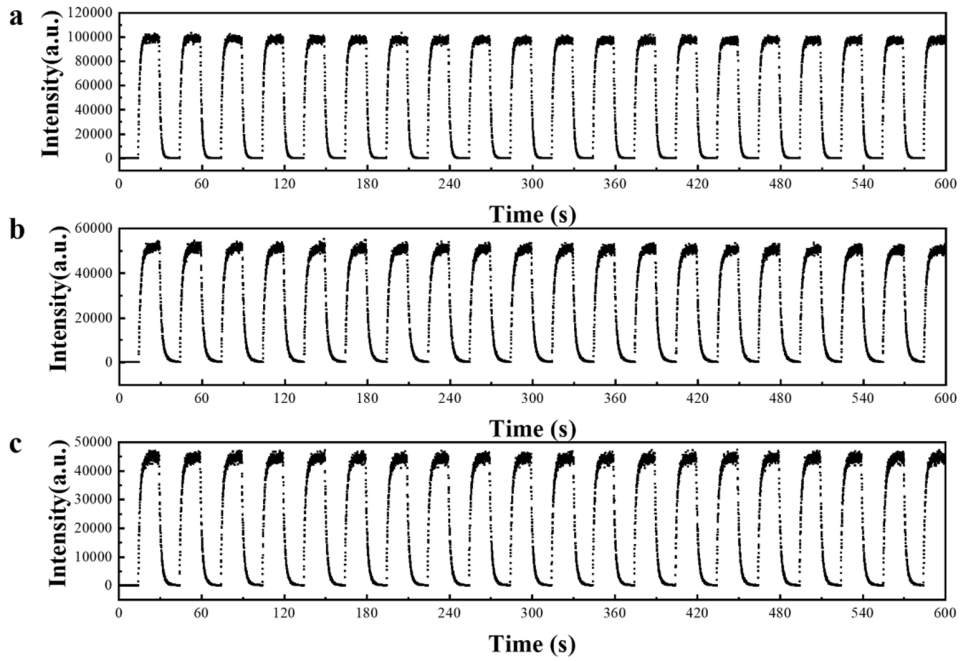

Fig. S27. (a) The cycle of PA@BA photo-activation and deactivation behavior during 600 seconds. (b) The cycle of TPA@BA photo-activation and deactivation behavior during 600 seconds. (c) The cycle of TA@BA photo-activation and deactivation behavior during 600 seconds.

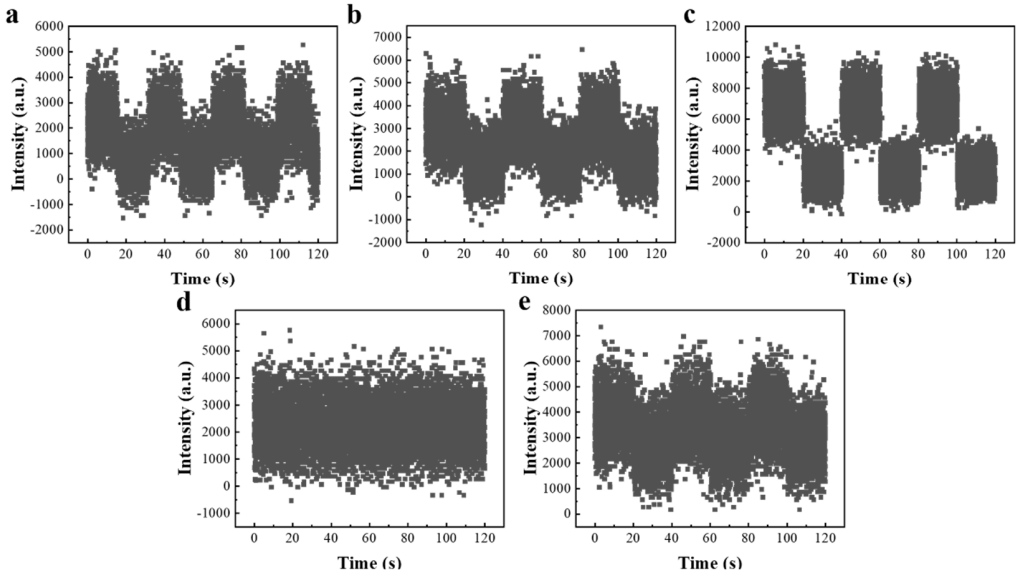

Fig. S28. (a) The cycle of pure BA during 120 seconds. (λ_{ex}=254 nm, 298 K) (b) The cycle of pure PA during 120 seconds. (λ_{ex}=254 nm, 298 K) (c) The cycle of pure IPA during 120 seconds.

(λ_{ex}=254 nm, 298 K) (d) The cycle of pure TPA during 120 seconds. (λ_{ex}=254 nm, 298 K) (e) The cycle of pure TA during 120 seconds, respectively. (λ_{ex}=254 nm, 298 K)

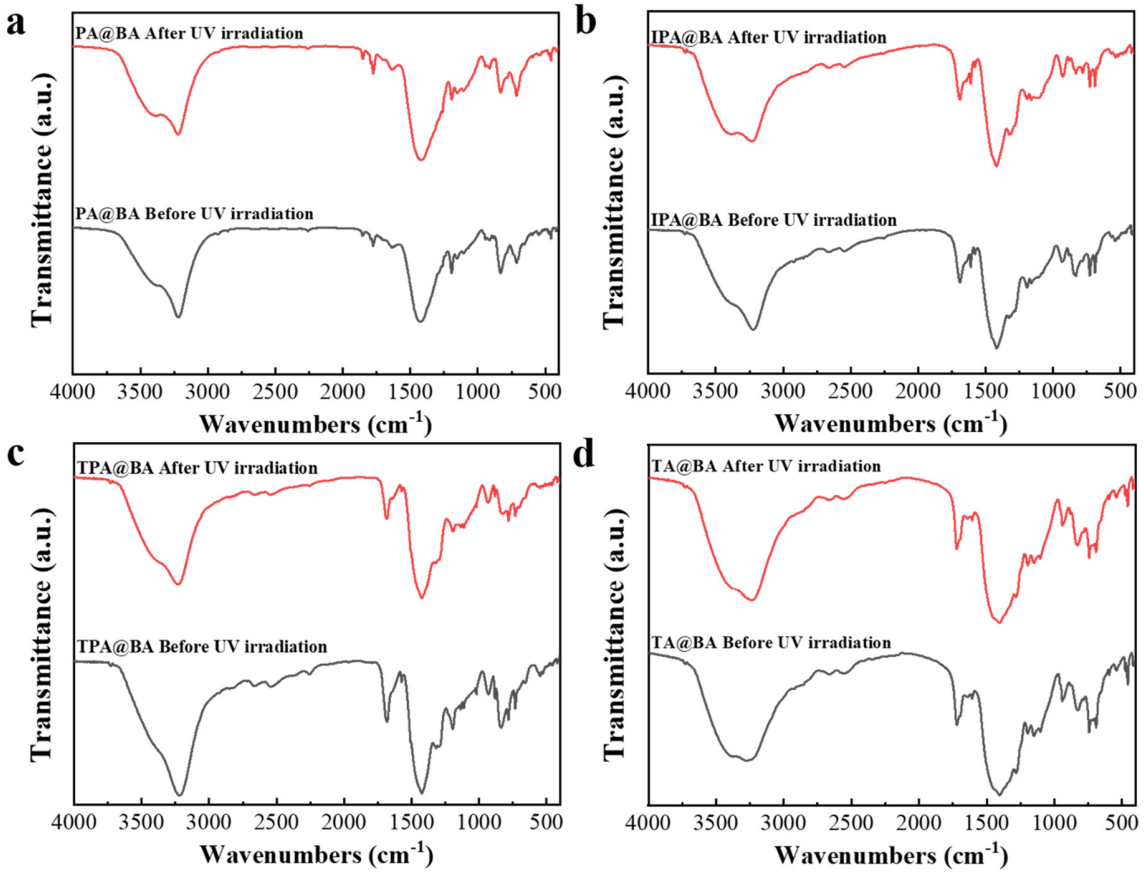

Fig. S29. The FT-IR spectra of BADs@BA before and after 12 h of continuous UV irradiation. (λ_{ex}=254 nm)

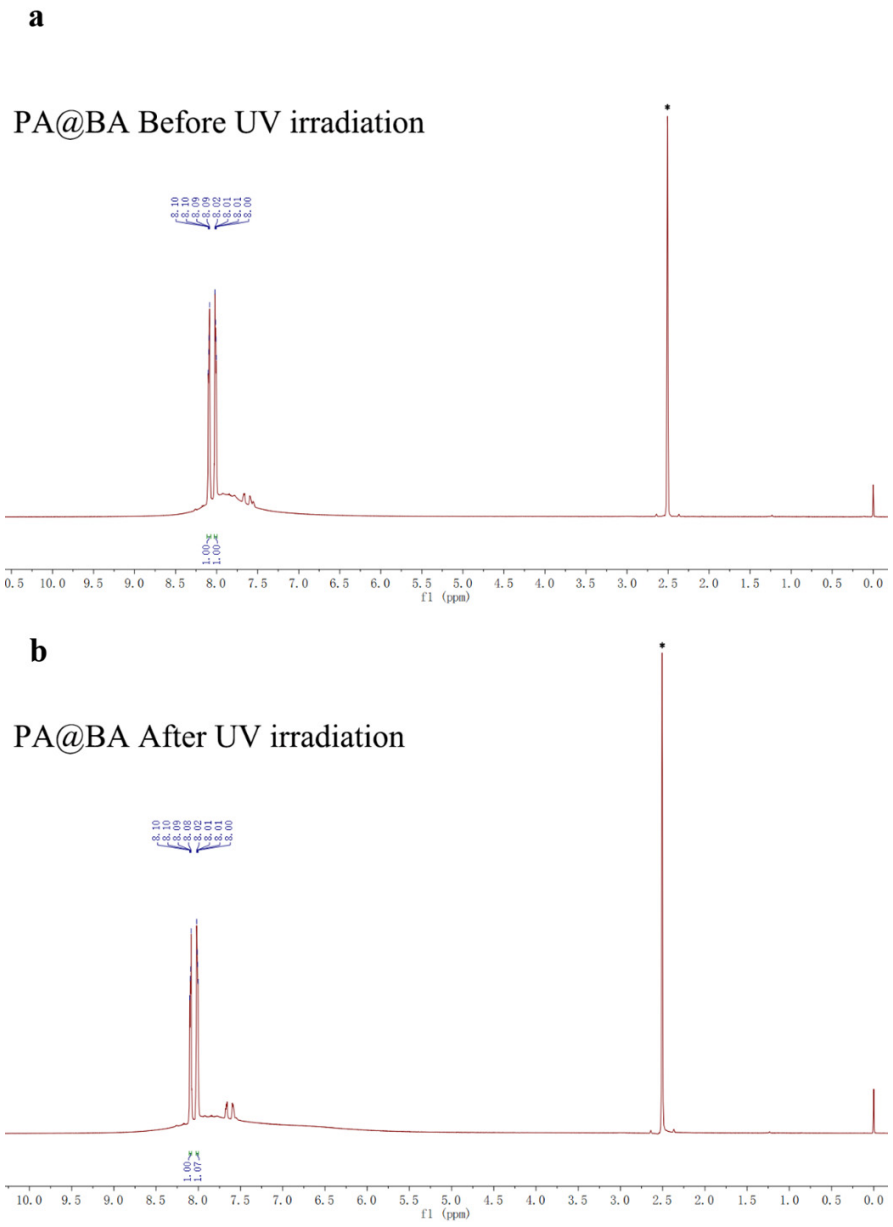

Fig. S30. (a) and (b) ^{1}H NMR spectra of the PA@BA before and after 12 h of continuous UV irradiation: ^{1}H NMR (400 MHz, DMSO-d_6) δ 8.09 (dd, J = 5.5, 3.2 Hz, 2H), 8.01 (dd, J = 5.5, 3.2 Hz, 2H). The solvent peaks were marked as asterisk.

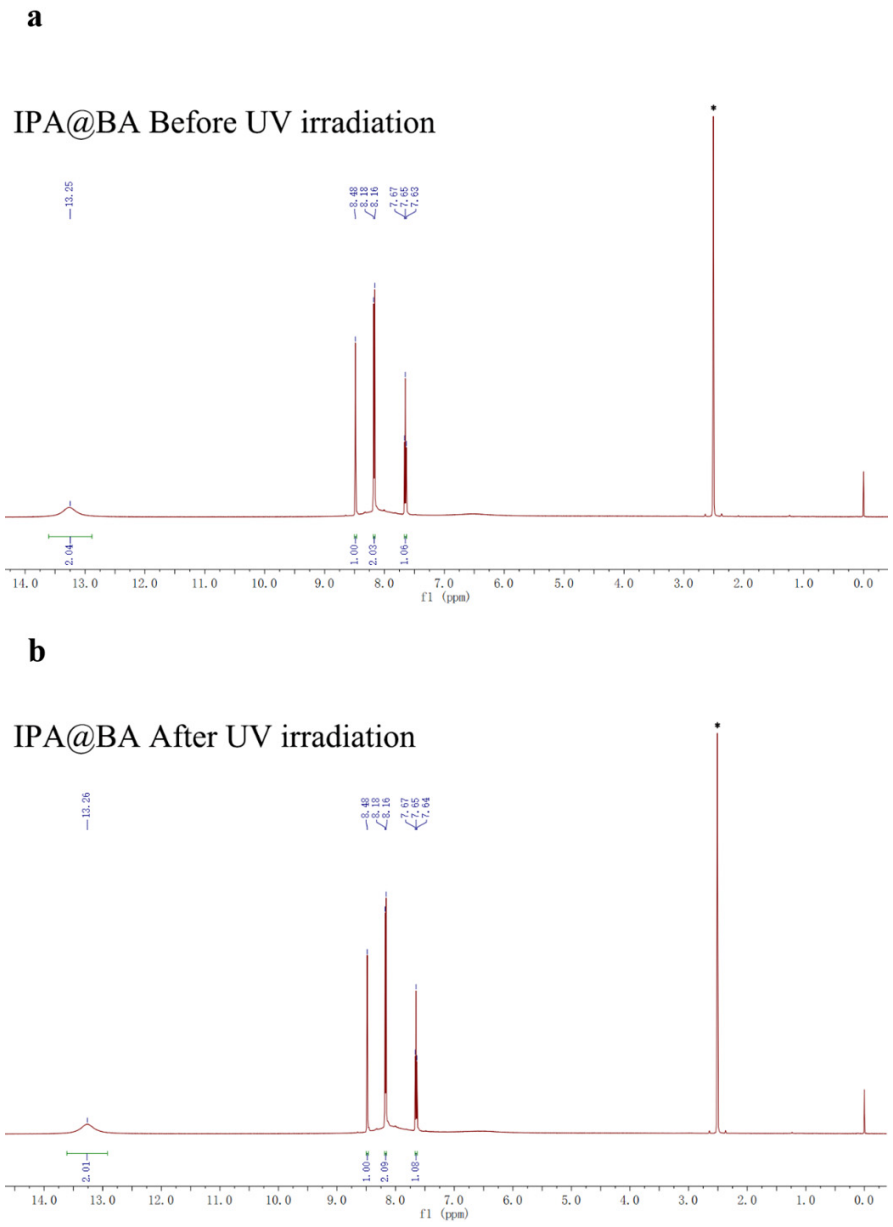

Fig. S31. (a) and (b) ^{1}H NMR spectra of the IPA@BA before and after 12 h of continuous UV irradiation: ^{1}H NMR (400 MHz, DMSO-d_6) δ 13.26 (s, 2H), 8.48 (s, 1H), 8.17 (d, J = 7.7 Hz, 2H), 7.65 (t, J = 7.7 Hz, 1H). The solvent peaks were marked as asterisk.

a

TPA@BA Before UV irradiation

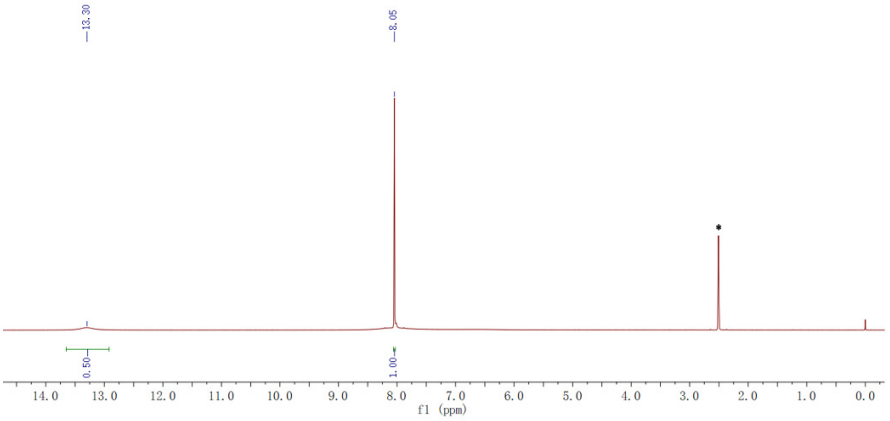

b

TPA@BA After UV irradiation

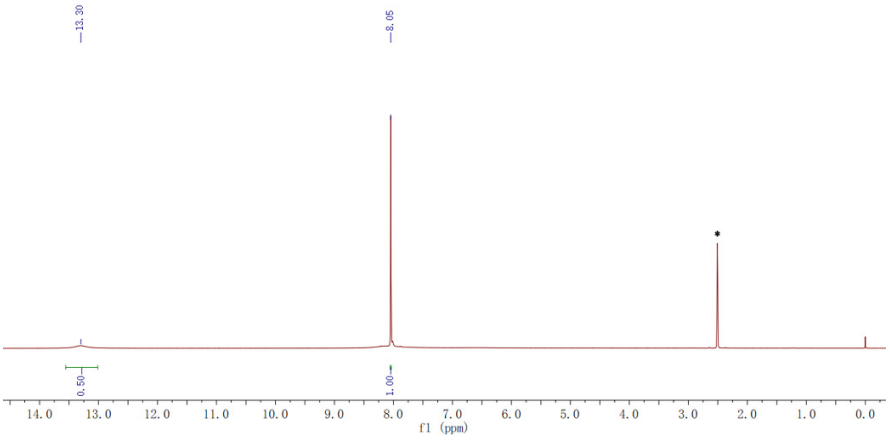

Fig. S32. (a) and (b) ^{1}H NMR spectra of the TPA@BA before and after 12 h of continuous UV irradiation: ^{1}H NMR (400 MHz, DMSO-d_6) δ 13.30 (s, 2H), 8.05 (d, J = 1.2 Hz, 4H). The solvent peaks were marked as asterisk.

a

TA@BA Before UV irradiation

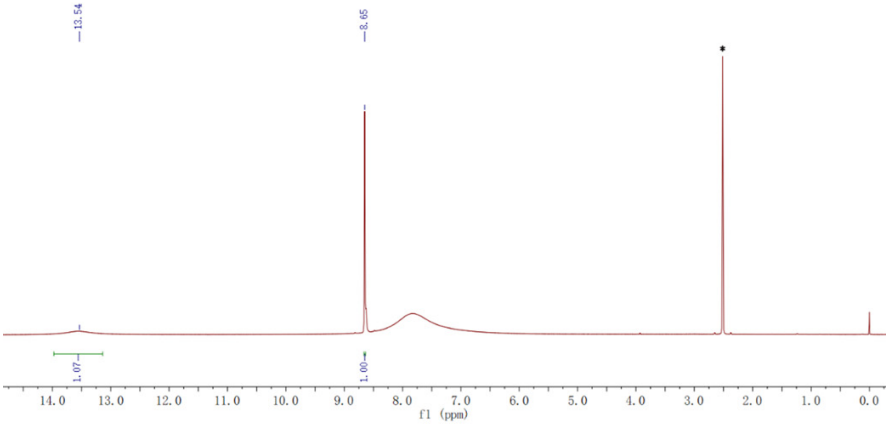

b

TA@BA After UV irradiation

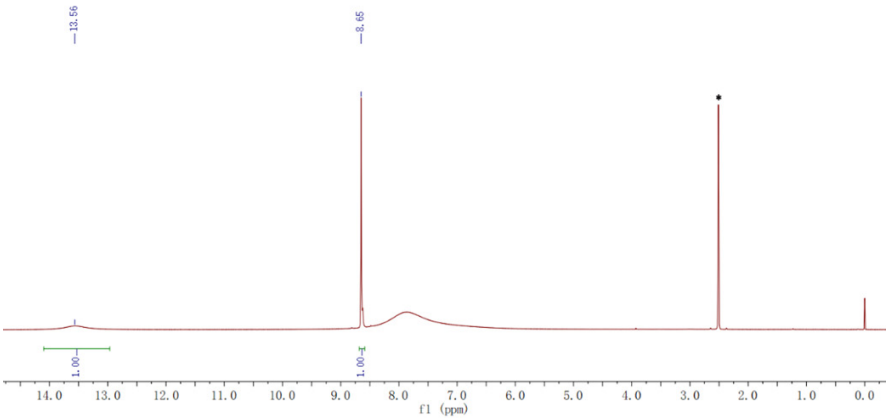

Fig. S33. (a) and (c) ^{1}H NMR spectra of the TA@BA before and after 12 h of continuous UV irradiation: ^{1}H NMR (400 MHz, DMSO-d_6) δ 13.54 (s, 3H), 8.65 (s, 3H). The solvent peaks were marked as asterisk.

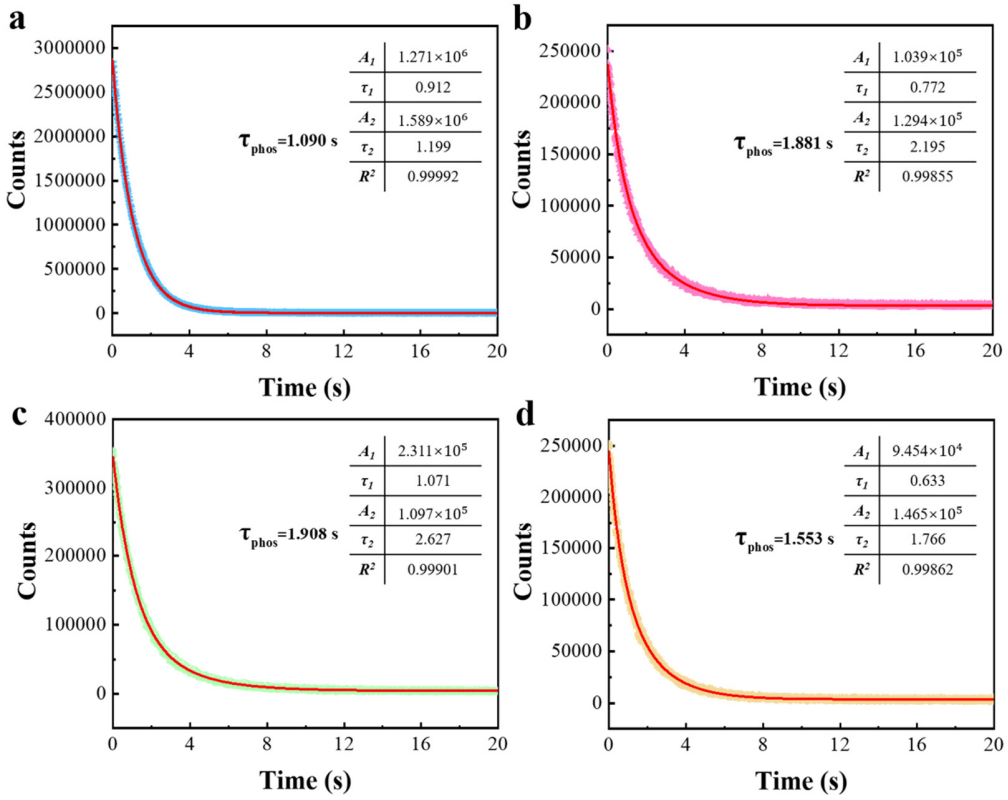

Fig. S34. (a) Lifetime decay profiles of PA@BA after photo-activation under ambient condition. (b) Lifetime decay profiles of IPA@BA after photo-activation under ambient condition. (c) Lifetime decay profiles of TPA@BA after photo-activation under ambient condition. (d) Lifetime decay profiles of TA@BA after photo-activation under ambient condition, respectively.

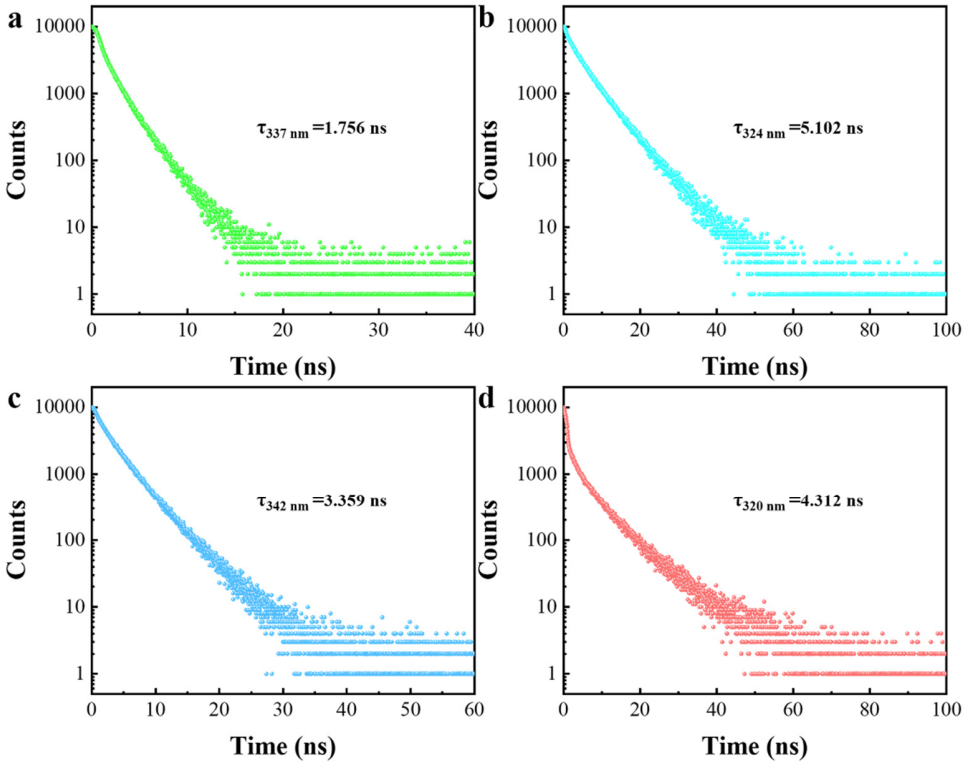

Fig. S35. (a) Fluorescence lifetime of PA@BA at 337 nm. (b) Fluorescence lifetime of IPA@BA at 324 nm. (c) Fluorescence lifetime of TPA@BA at 342 nm. (d) Fluorescence lifetime of TA@BA at 320 nm.

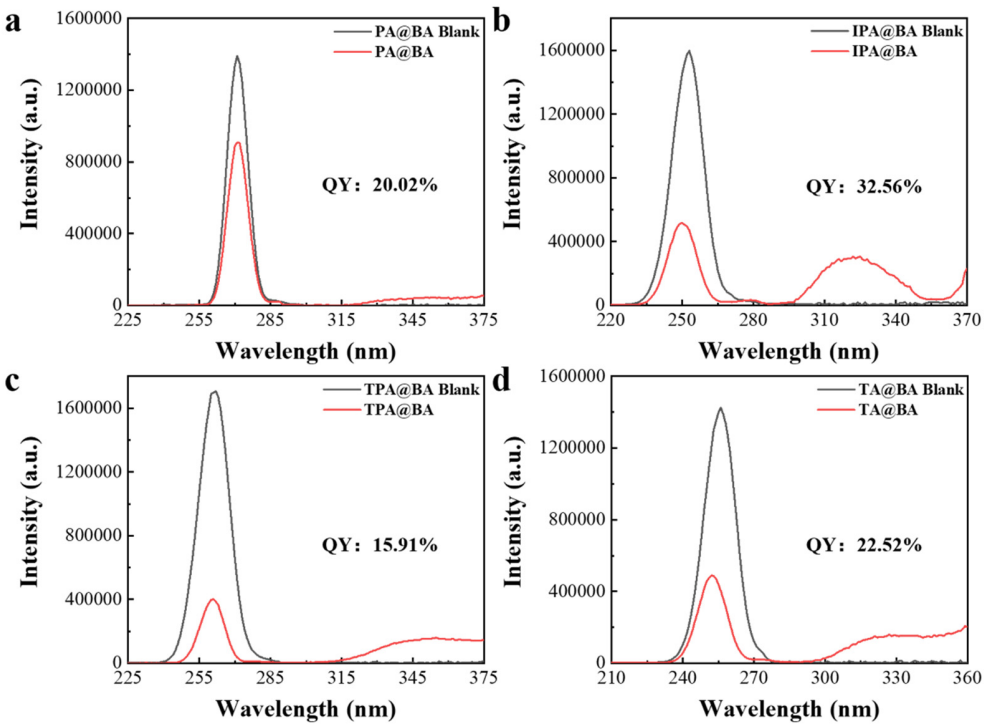

Fig. S36. (a) The fluorescence quantum yield spectra of PA@BA (measurement range: 225 ~ 375 nm; fluorescence range: 315 ~ 375 nm). (b) The fluorescence quantum yield spectra of IPA@BA (measurement range: 220 ~ 370 nm; fluorescence range: 295 ~ 355 nm). (c) The fluorescence quantum yield spectra of TPA@BA (measurement range: 225 ~ 375 nm; fluorescence range: 310 ~ 375 nm). (d) The fluorescence quantum yield spectra of TA@BA (measurement range: 210 ~ 360 nm; fluorescence range: 295 ~ 355 nm).

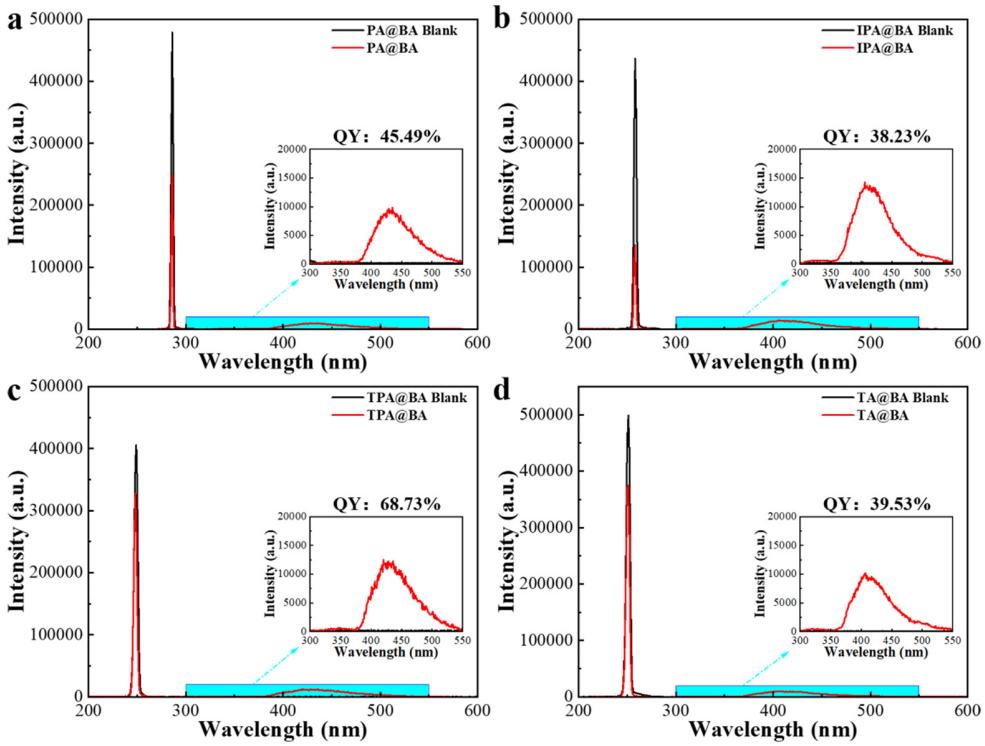

Fig. S37. (a) The phosphorescence quantum yield spectra of PA@BA (measurement range: 200 ~ 600 nm; phosphorescence: 375 ~ 550 nm). (b) The phosphorescence quantum yield spectra of IPA@BA (measurement range: 200 ~ 600 nm; phosphorescence: 370 ~ 550 nm). (c) The phosphorescence quantum yield spectra of TPA@BA (measurement range: 200 ~ 600 nm; phosphorescence: 375 ~ 550 nm). (d) The phosphorescence quantum yield spectra of TA@BA (measurement range: 200 ~ 600 nm; phosphorescence: 355 ~ 550 nm).

Table S2. The absolute fluorescence and phosphorescence quantum yields of photo-activated BADs@BA under excitation light.

Sample	λ_{ex}/nm [a]	λ_f/nm [b]	λ_p/nm [c]	τ_f/ns [d]	τ_p/s [e]	Φ_f [f]	Φ_p [g]
PA@BA	286	337	434	1.756	1.071	20.02%	45.49%
IPA@BA	258	324	404	5.102	1.881	32.56%	38.23%
TPA@BA	248	342	429	3.359	1.908	15.91%	68.73%
TA@BA	250	320	407	4.312	1.553	22.52%	39.53%

[a]: Excitation wavelength; ***[b]***: Fluorescence emission wavelength; ***[c]***: Phosphorescence emission wavelength; ***[d]***: Fluorescence lifetime; ***[e]***: Phosphorescence lifetime; ***[f]***: Absolute fluorescence quantum yield (without phosphorescence emission); ***[g]***: Absolute phosphorescence quantum yield (without fluorescence emission).

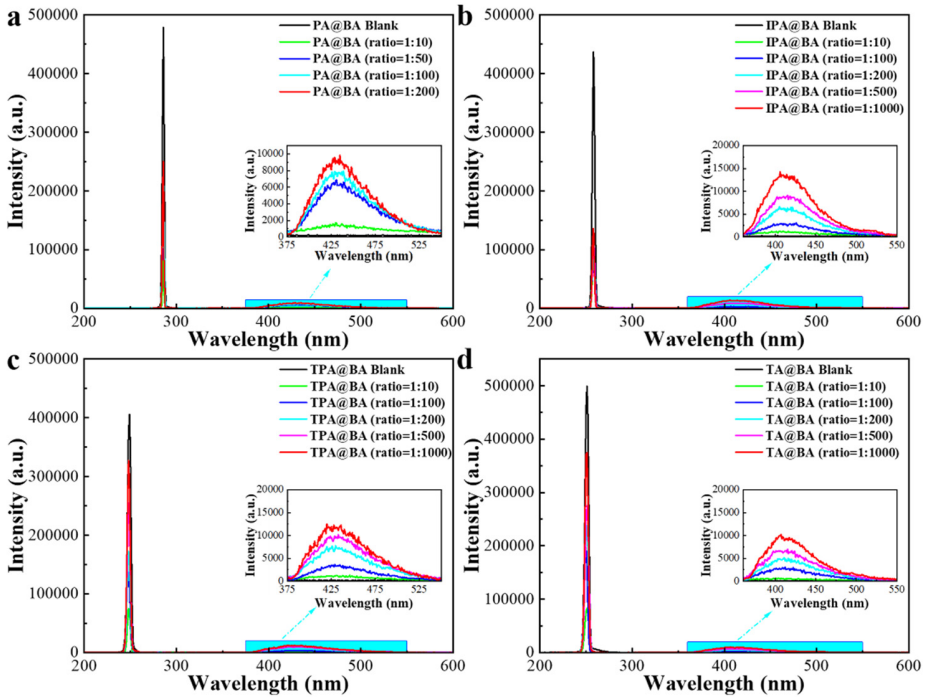

Fig. S38. (a) The phosphorescence quantum yield spectra of PA@BA at different ratios. (b) The phosphorescence quantum yield spectra of IPA@BA at different ratios. (c) The phosphorescence quantum yield spectra of TPA@BA at different ratios. (d) The phosphorescence quantum yield spectra of TA@BA at different ratios.

Table S3. The absolute phosphorescence quantum yields of BADs@BA at different doped ratios.

Ratio (n_{BADs} : n_{BA})	Φ_p [a] PA@BA	Φ_p IPA@BA	Φ_p TPA@BA	Φ_p TA@BA
1 : 10	3.020%	2.480%	2.240%	1.140%
1 : 50	29.77%	-	-	-
1 : 100	40.25%	7.370%	7.290%	6.050%
1 : 200	45.49%	17.11%	18.48%	13.09%
1 : 500	-	29.99%	35.68%	19.82%
1 : 1000	-	38.23%	68.73%	39.53%

[a]: Absolute phosphorescence quantum yield.

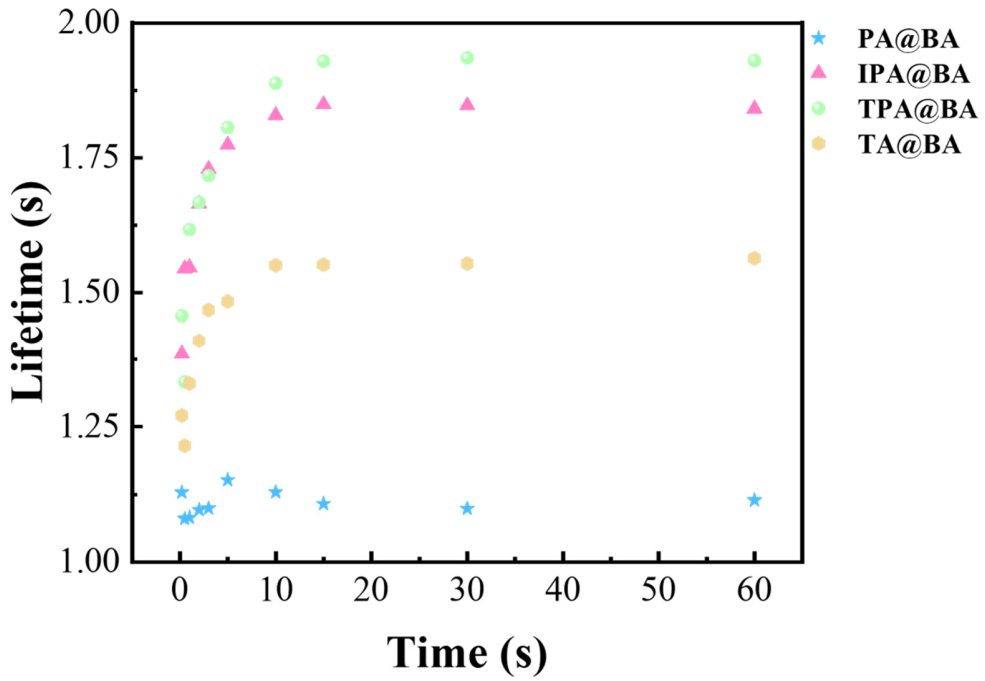

Fig. S39. The phosphorescence lifetimes of BADs@BA after different irradiation times ranging from 0.2 to 60 seconds under ambient conditions.

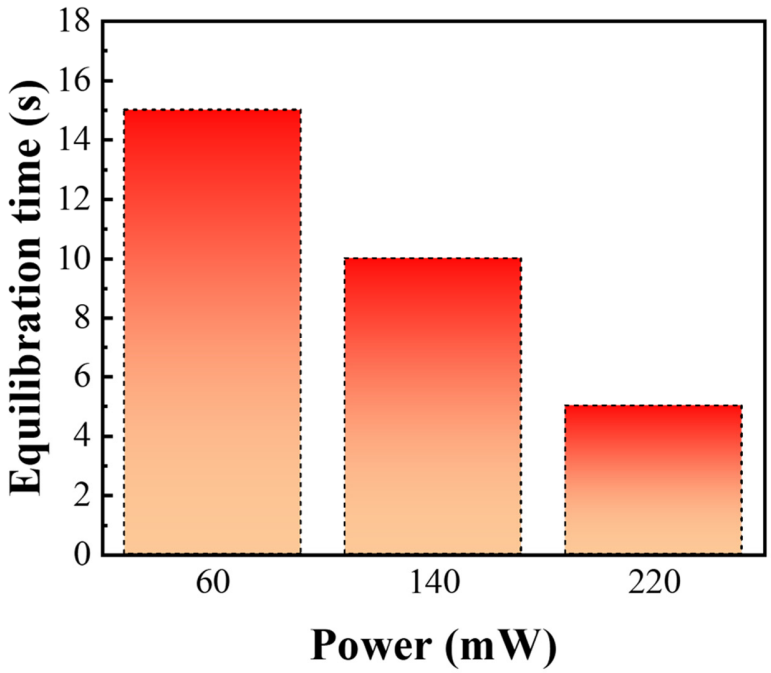

Fig. S40. The equilibration photo-activation time of BADs@BA under different excitation power.

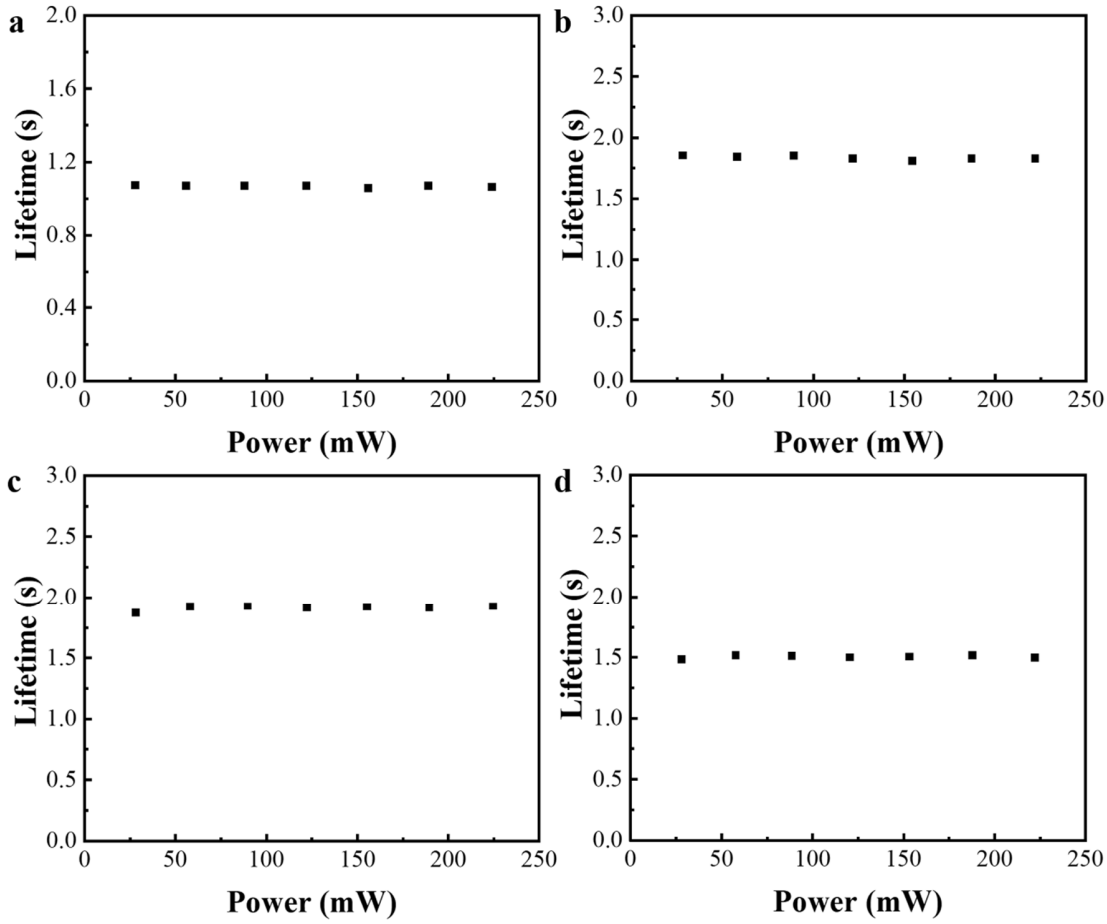

Fig. S41. (a) The lifetimes of PA@BA under different excitation light power. (b) The lifetimes of IPA@BA under different excitation light power. (c) The photo-activation lifetimes of TPA@BA under different excitation light power. (d) the lifetimes of TA@BA under different excitation light power, respectively.

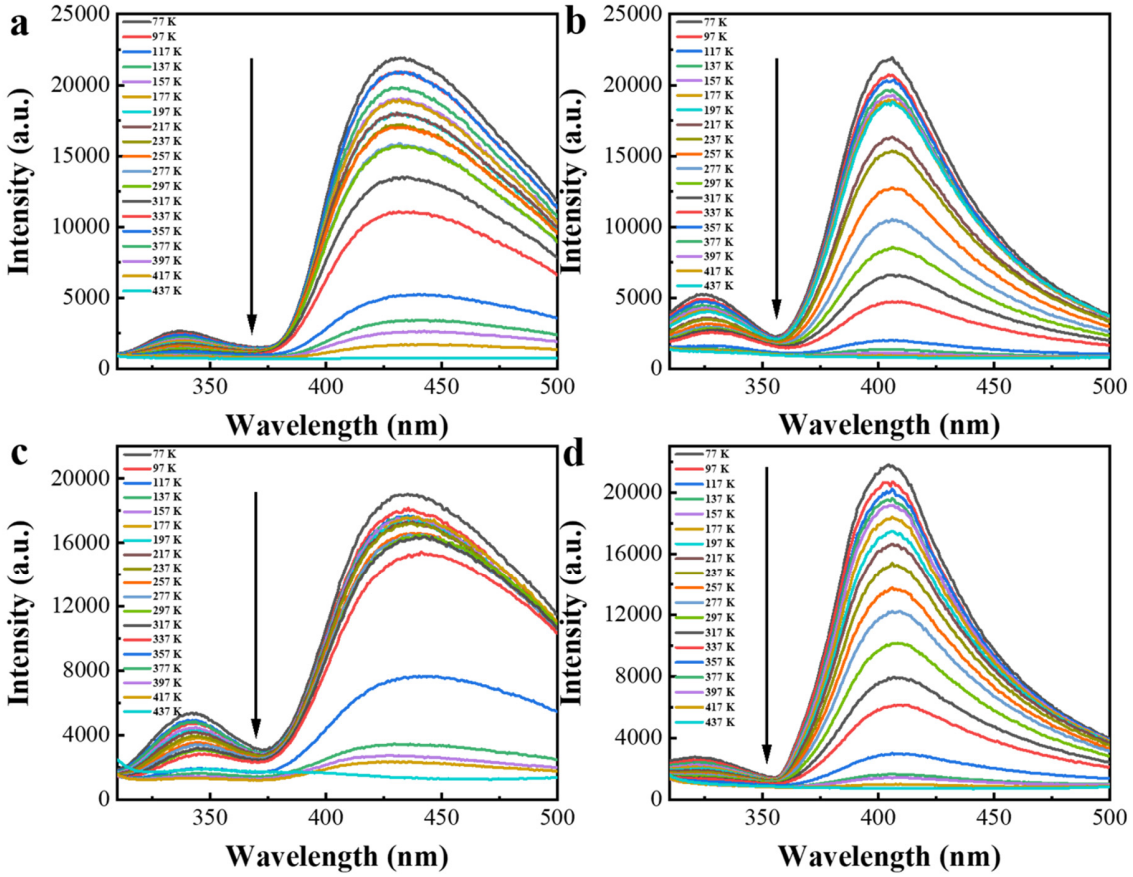

Fig. S42. (a) Temperature-dependent fluorescence spectra of PA@BA from 77 K to 437 K. (b) Temperature-dependent fluorescence spectra of IPA@BA from 77 K to 437 K. (c) Temperature-dependent fluorescence spectra of TPA@BA from 77 K to 437 K. (d) Temperature-dependent fluorescence spectra of TA@BA from 77 K to 437 K.

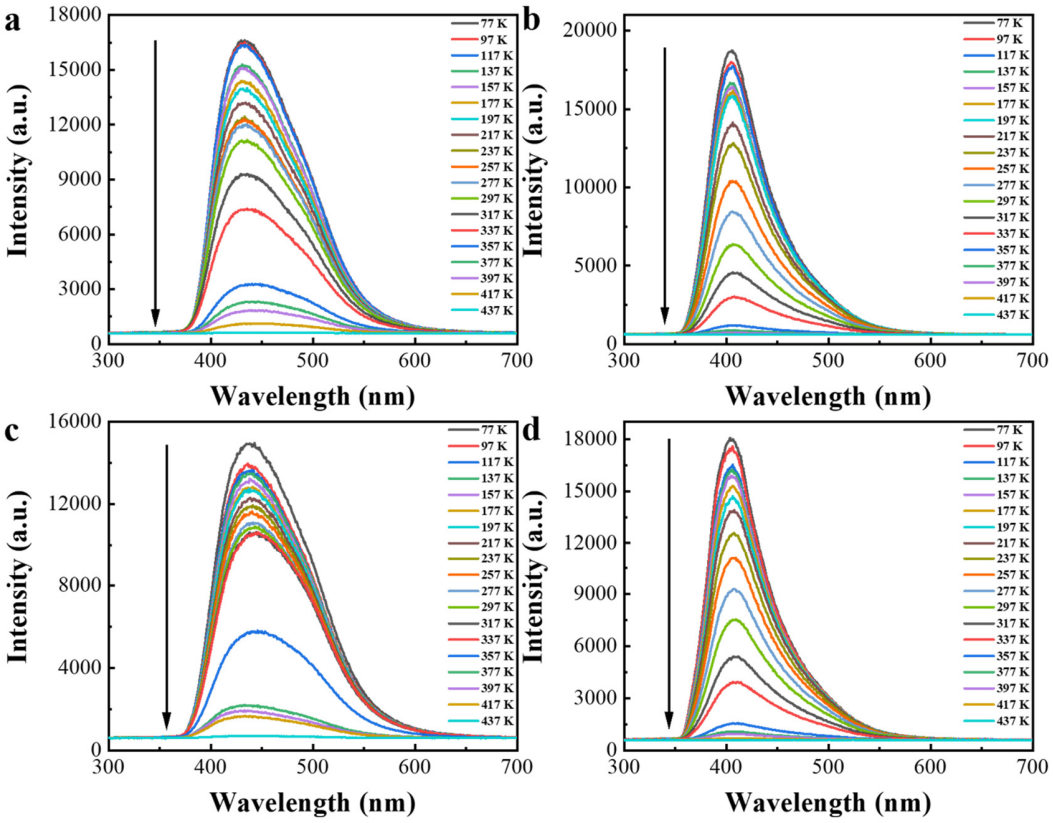

Fig. S43. (a) Temperature-dependent phosphorescence spectra of PA@BA from 77 K to 437 K. (b) Temperature-dependent phosphorescence spectra of IPA@BA from 77 K to 437 K. (c) Temperature-dependent phosphorescence spectra of TPA@BA from 77 K to 437 K. (d) Temperature-dependent phosphorescence spectra of TA@BA from 77 K to 437 K.

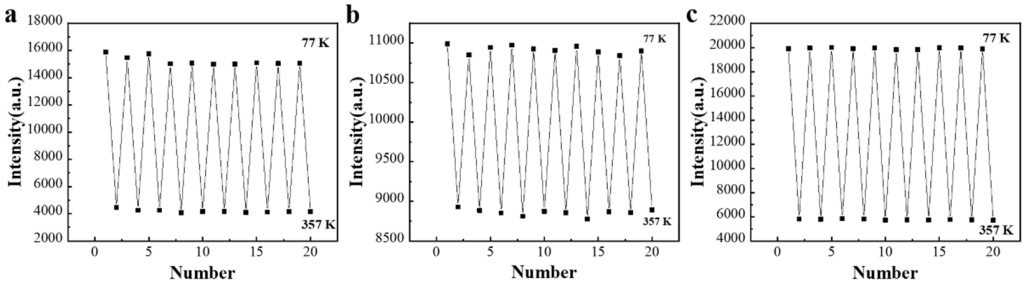

Fig. S44. (a) The temperature cyclicality of PA@BA between 77 K and 357 K. (b) The temperature cyclicality of TPA@BA between 77 K and 357 K. (c) The temperature cyclicality of TA@BA between 77 K and 357 K.

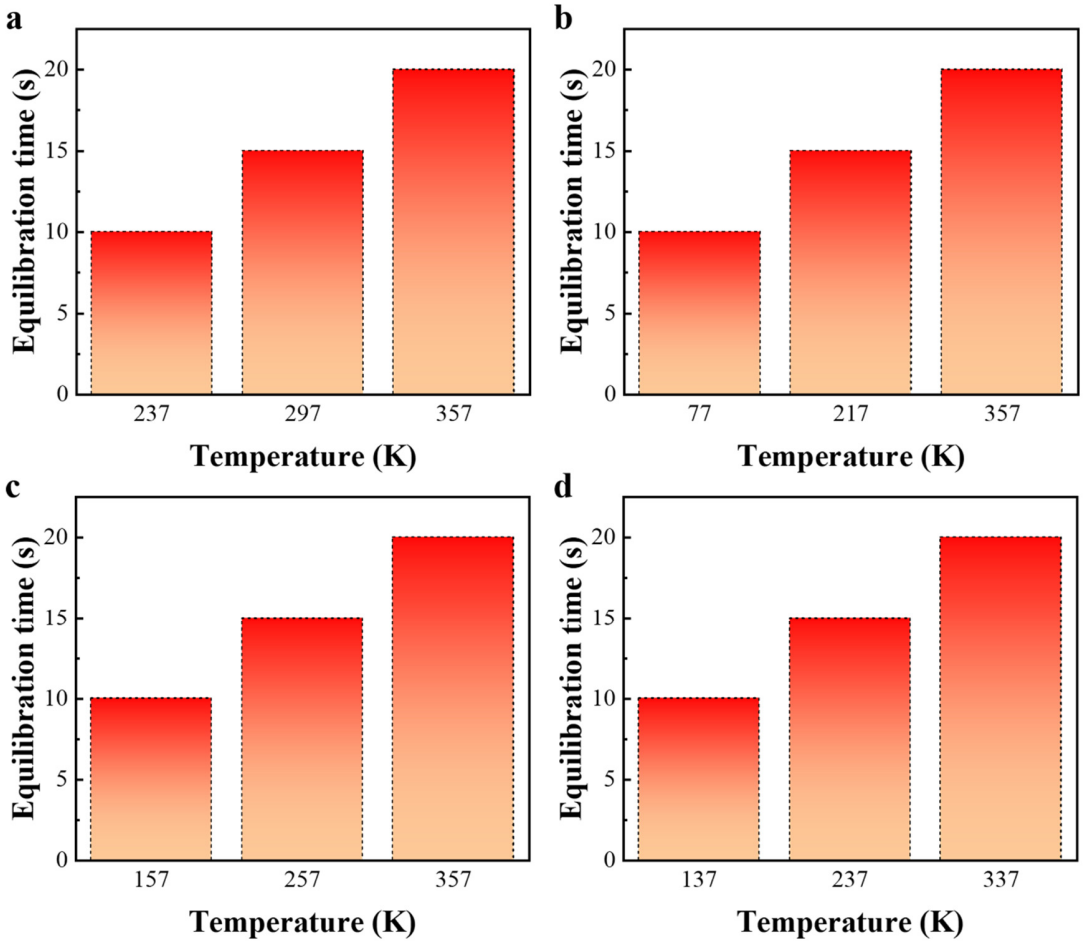

Fig. S45. (a) The equilibration photo-activation time of PA@BA under different temperature. (b) The equilibration photo-activation time of IPA@BA under different temperature. (c) The equilibration photo-activation time of TPA@BA under different temperature. (d) The equilibration photo-activation time of TA@BA under different temperature, respectively.

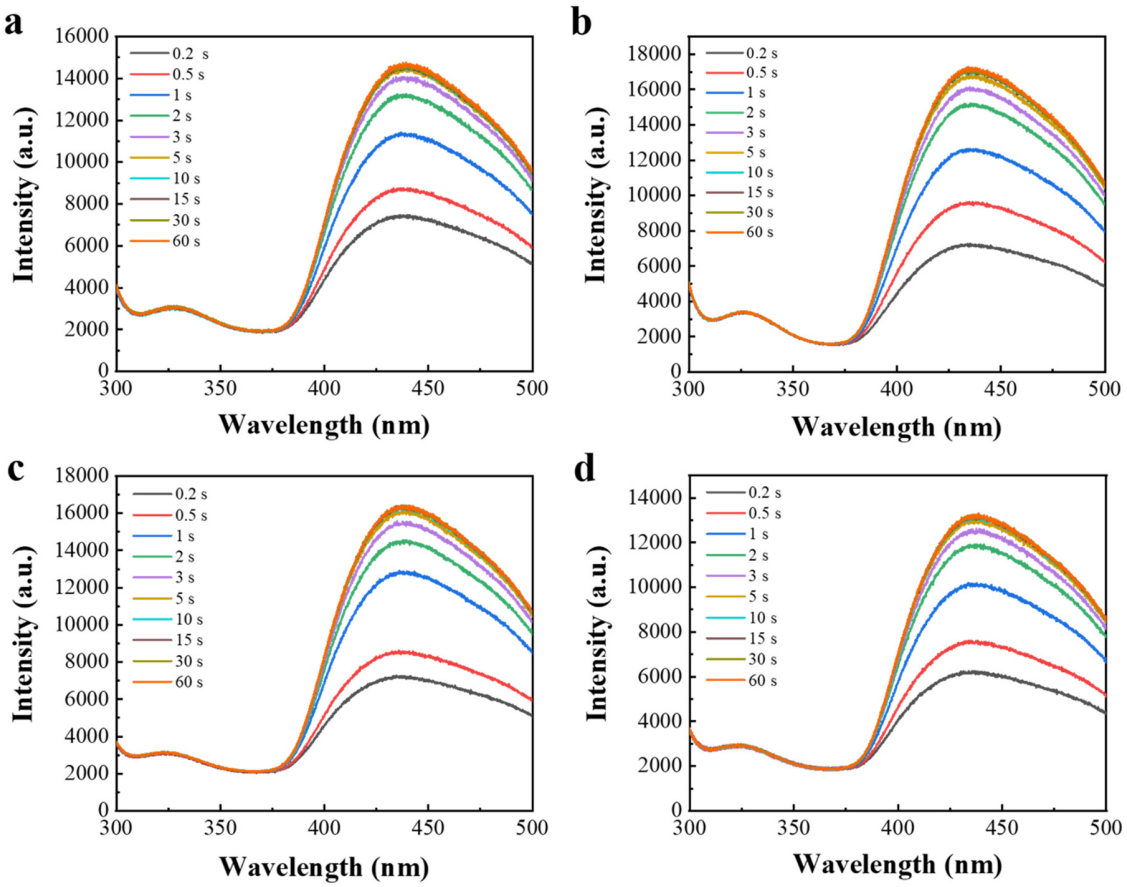

Fig. S46. (a), (b), (c) and (d) fluorescence spectra of PA@BA under ambient, vacuum, nitrogen and oxygen atmosphere at different irradiation time.

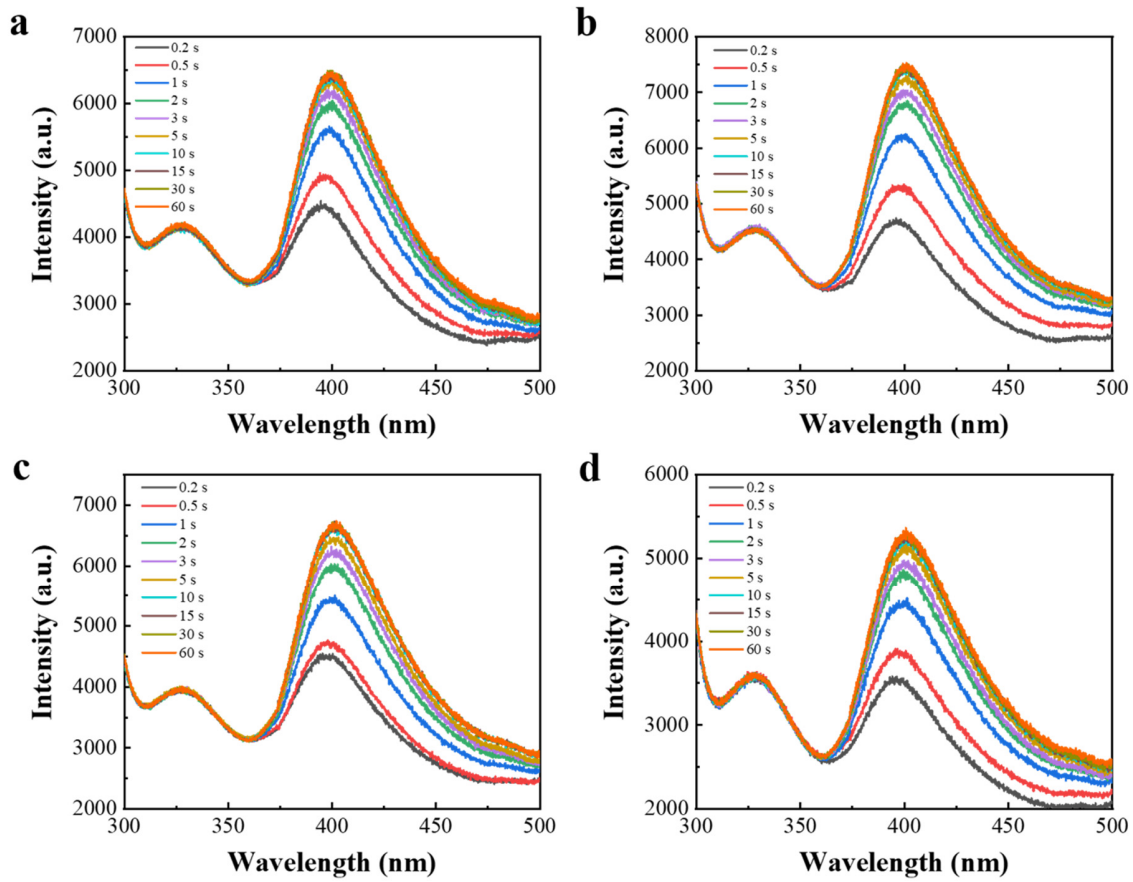

Fig. S47. (a), (b), (c) and (d) fluorescence spectra of IPA@BA under ambient, vacuum, nitrogen and oxygen atmosphere at different irradiation time.

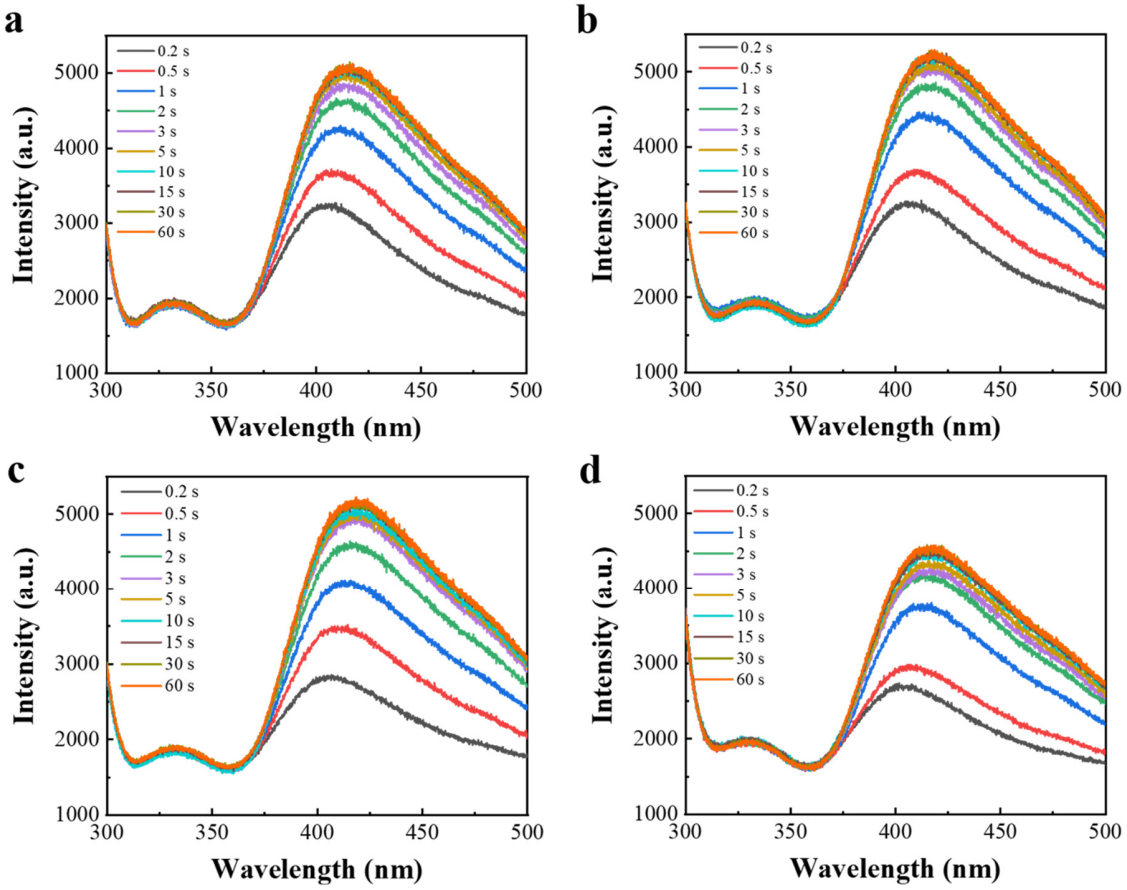

Fig. S48. (a), (b), (c) and (d) fluorescence spectra of TPA@BA under ambient, vacuum, nitrogen and oxygen atmosphere at different irradiation time.

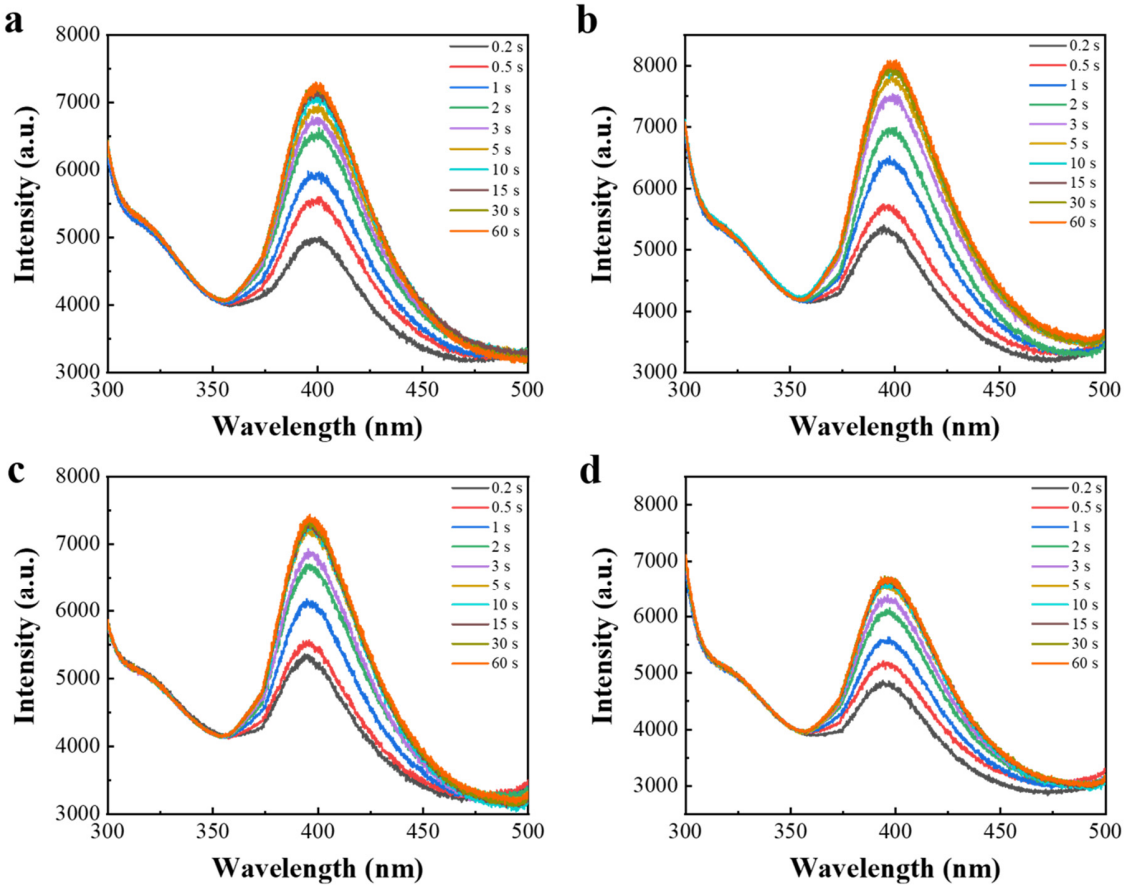

Fig. S49. (a), (b), (c) and (d) fluorescence spectra of TA@BA under ambient, vacuum, nitrogen and oxygen atmosphere at different irradiation time.

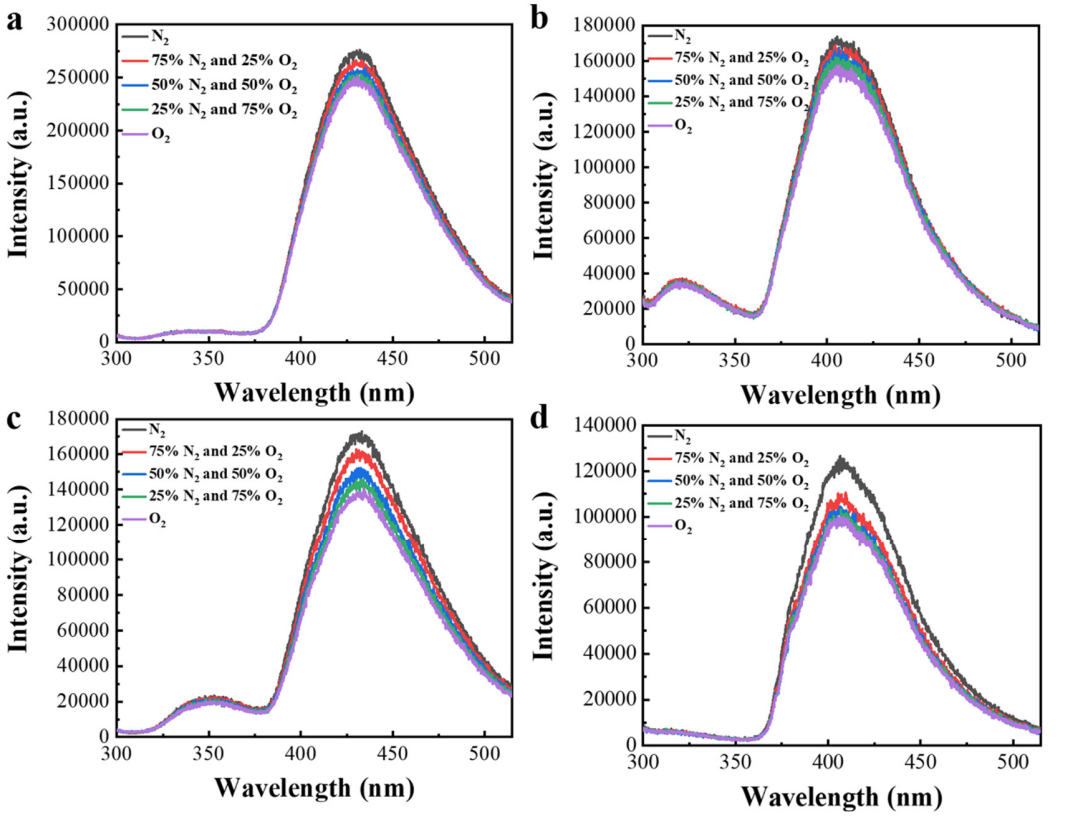

Fig. S50. (a) The fluorescence spectra of PA@BA under oxygen with different concentrations; (b) The fluorescence spectra of IPA@BA under oxygen with different concentrations; (c) The fluorescence spectra of TPA@BA under oxygen with different concentrations; (d) The fluorescence spectra of TA@BA under oxygen with different concentrations.

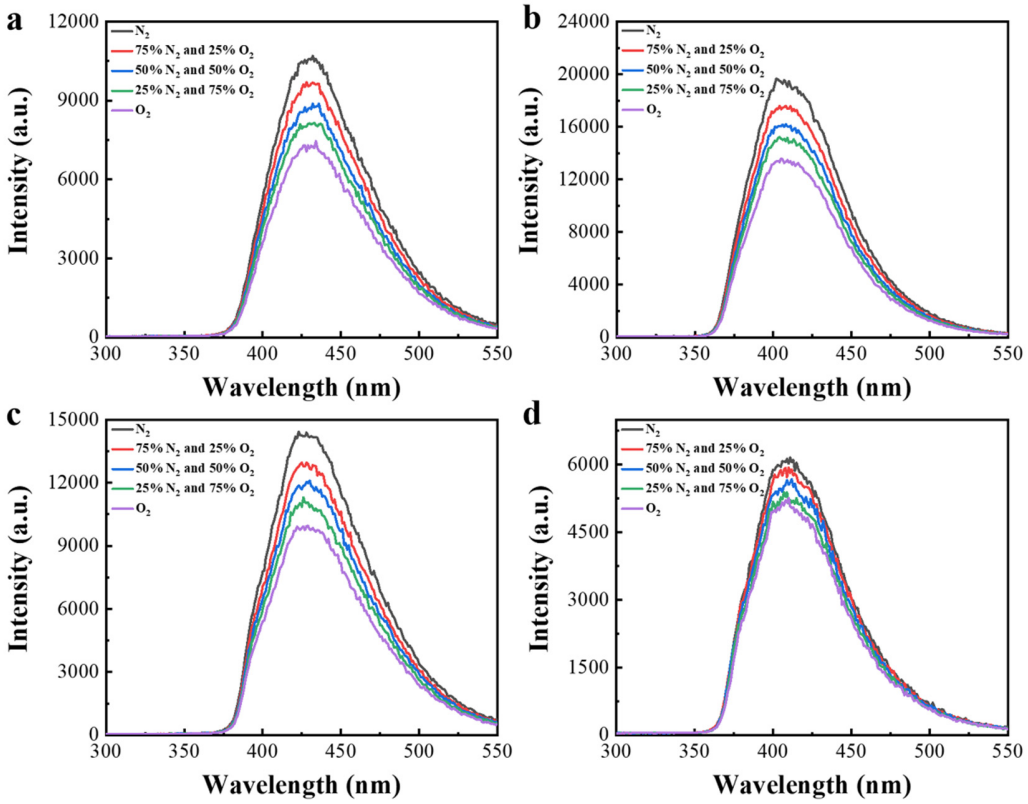

Fig. S51. (a) The phosphorescence spectra of PA@BA under oxygen with different concentrations; (b) The phosphorescence spectra of IPA@BA under oxygen with different concentrations; (c) The phosphorescence spectra of TPA@BA under oxygen with different concentrations; (d) The phosphorescence spectra of TA@BA under oxygen with different concentrations.

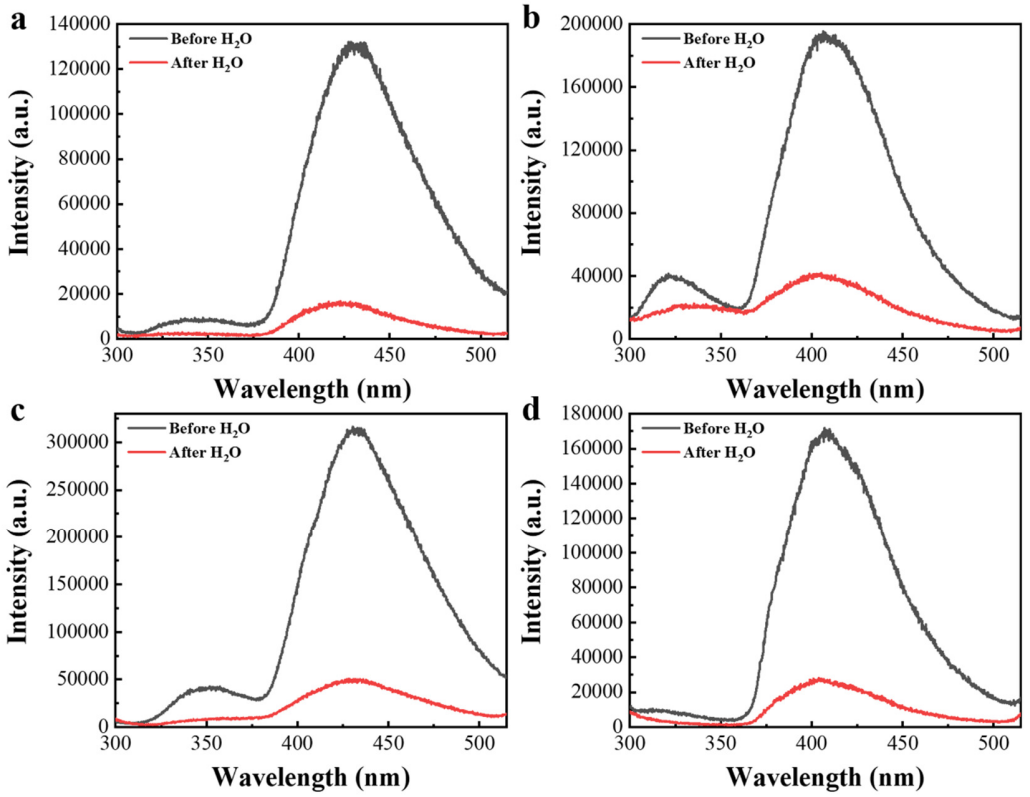

Fig. S52. (a) The fluorescence spectra of PA@BA before and after H_2O steam fumigation for 30 minutes; (b) The fluorescence spectra of IPA@BA before and after H_2O steam fumigation for 30 minutes; (c) The fluorescence spectra of TPA@BA before and after H_2O steam fumigation for 30 minutes; (d) The fluorescence spectra of TA@BA before and after H_2O steam fumigation for 30 minutes.

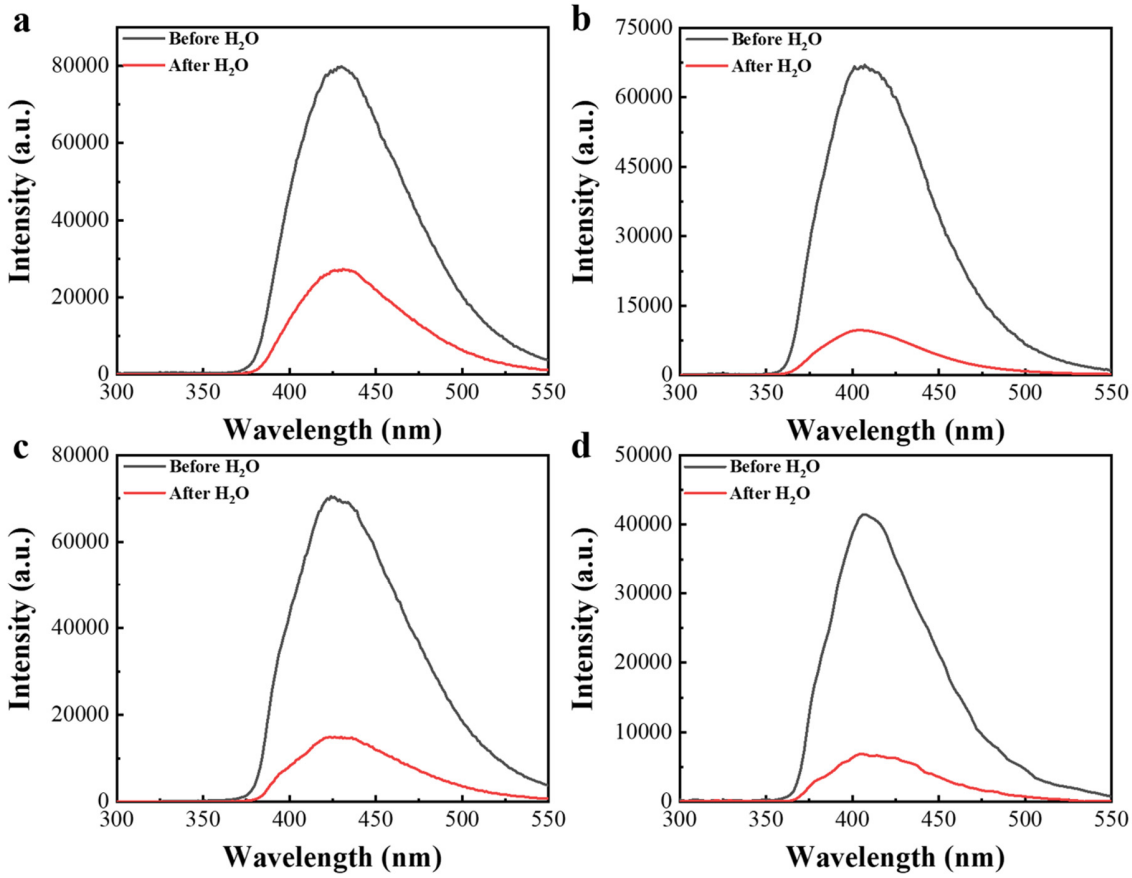

Fig. S53. (a) The phosphorescence spectra of PA@BA before and after H_2O steam fumigation for 30 minutes; (b) The phosphorescence spectra of IPA@BA before and after H_2O steam fumigation for 30 minutes; (c) The phosphorescence spectra of TPA@BA before and after H_2O steam fumigation for 30 minutes; (d) The phosphorescence spectra of TA@BA before and after H_2O steam fumigation for 30 minutes.

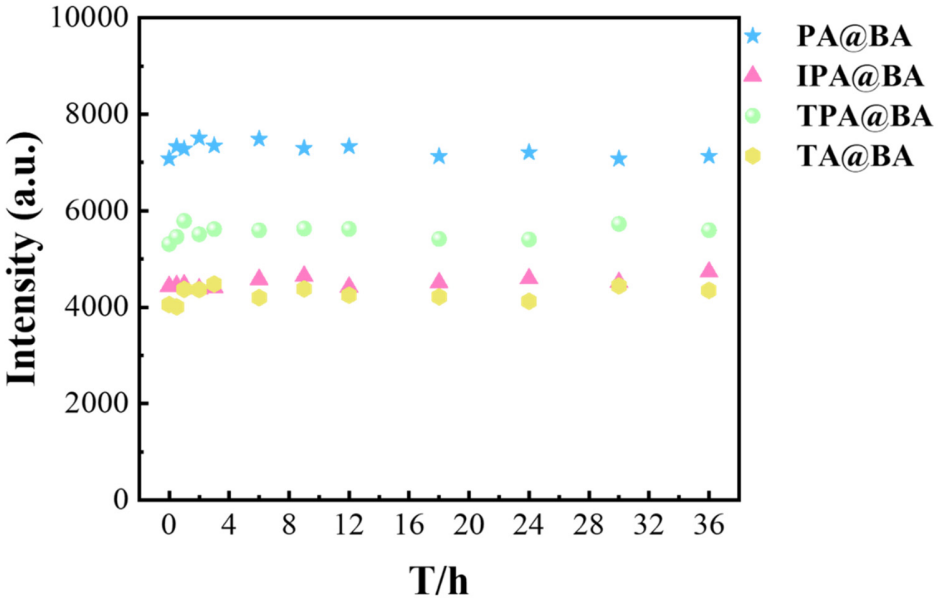

Fig. S54. The phosphorescence intensities of BADs@BA during 36 hours of continuous irradiation.

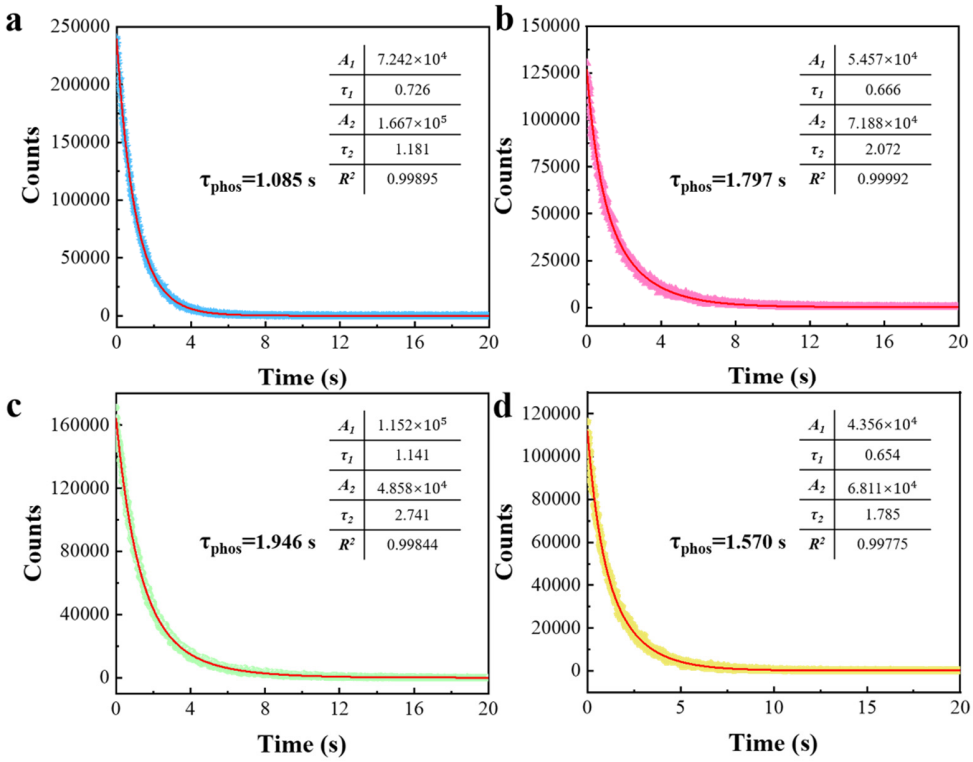

Fig. S55. (a) The phosphorescence lifetime of PA@BA after continuous irradiation for 36 hours. (b) The phosphorescence lifetime of IPA@BA after continuous irradiation for 36 hours. (c) The

phosphorescence lifetime of TPA@BA after continuous irradiation for 36 hours. (d) The phosphorescence lifetime of TA@BA after continuous irradiation for 36 hours.

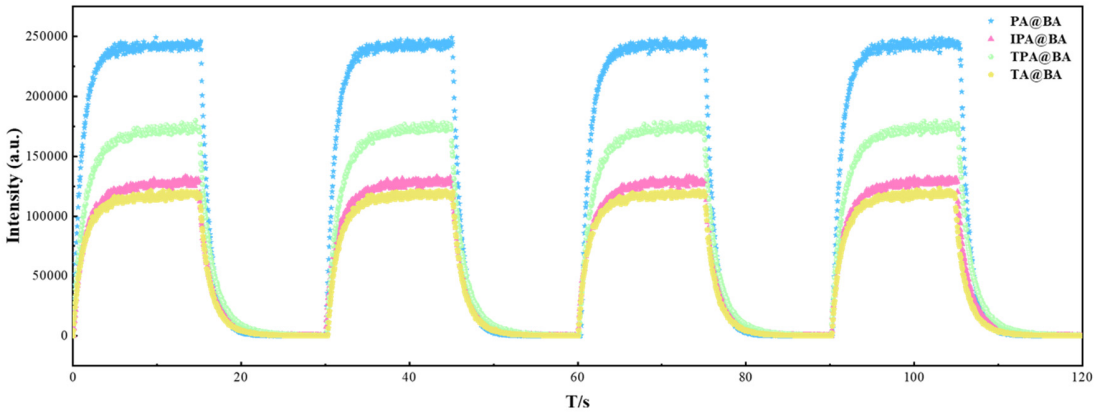

Fig. S56. The cycles of photo-activation and deactivation behaviour of BADs@BA after continuous irradiation for 36 hours.

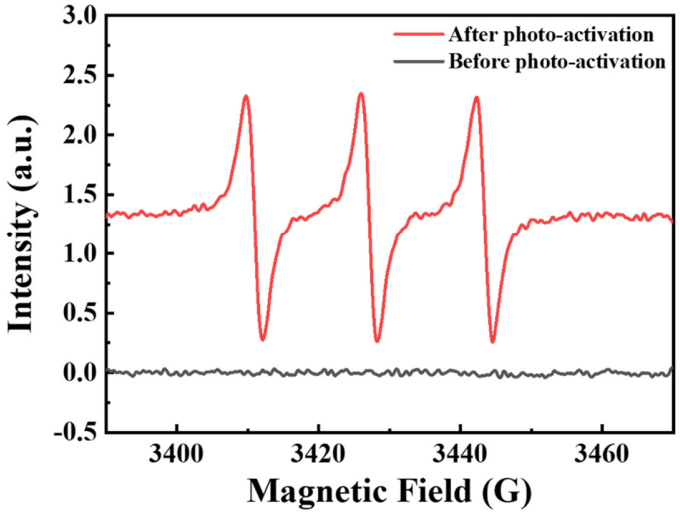

Fig. S57. The electron spin resonance (ESR) spectra of IPA@BA before and after the 254 nm UV irradiated 2 min.

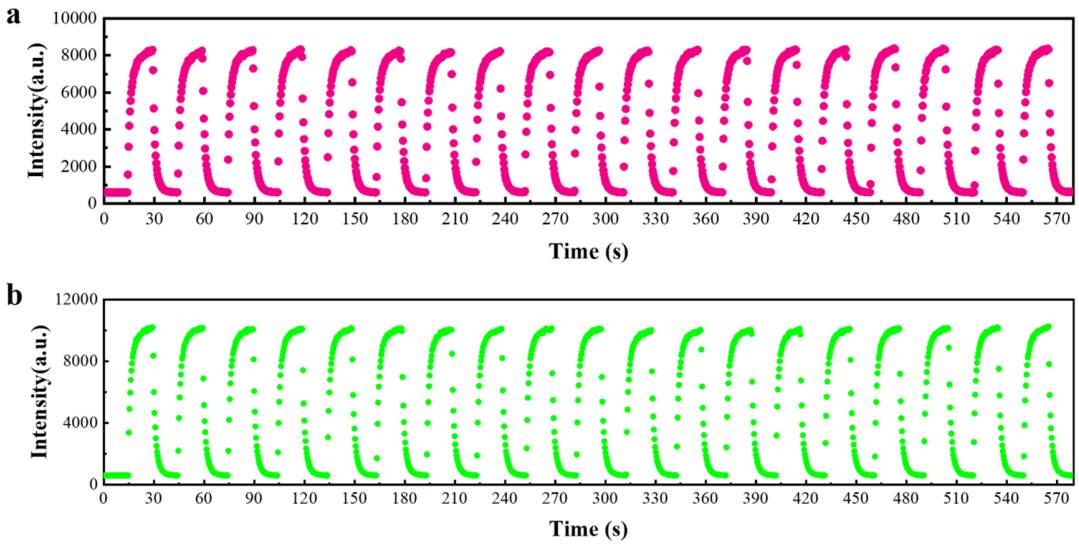

Fig. S58. The photo-activation cycles of IPA@BA (a) before 254 nm UV irradiation and (b) after 3 hours 254 nm UV irradiation. Both processes were carried out in vacuum condition.

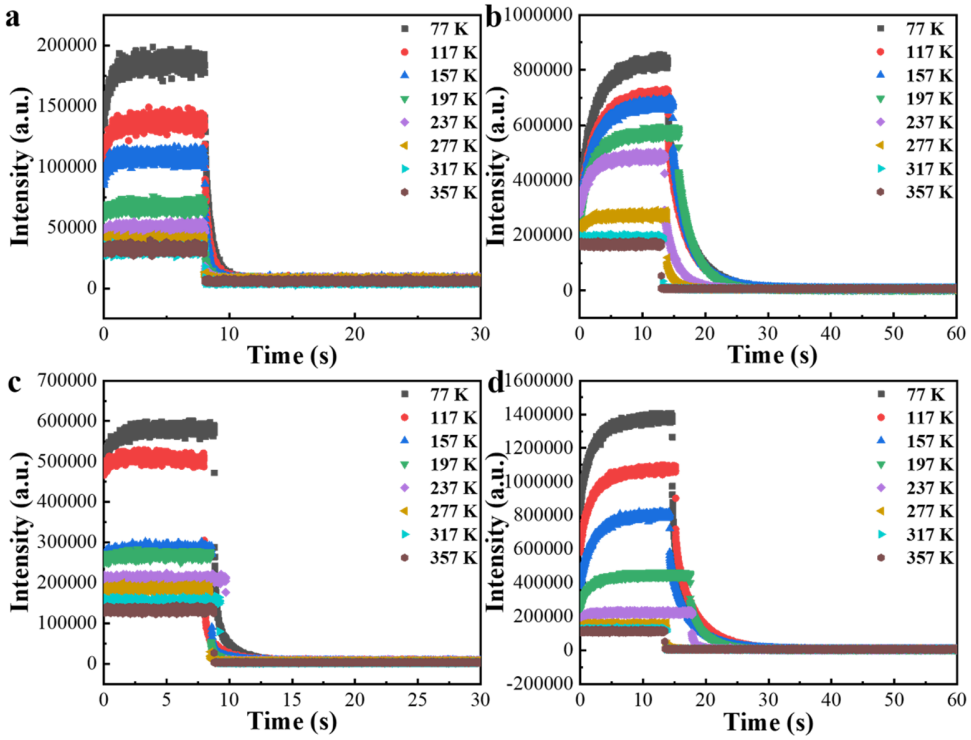

Fig. S59. (a) The photo-activation processes of pure PA under different temperature. (b) The photo-activation processes of pure IPA under different temperature. (c) The photo-activation

processes of pure TPA under different temperature. (d) The photo-activation processes of pure TA under different temperature, respectively.

Table S4. Crystallographic data of pristine and irradiated IPA single crystals.

Compound	**Pristine IPA**	**Irradiated IPA**
Formula	$C_8H_6O_4$	$C_8H_6O_4$
Formula weight (g mol^{-1})	166.13	166.13
Temperature (k)	298	100
Crystal color	colorless	colorless
Space group	P 21/c	P 21/c
a (Å)	3.6820(1)	3.6825(1)
b (Å)	16.3668(4)	16.3666(4)
c (Å)	11.6126(3)	11.6128(3)
α (deg)	90	90
β (deg)	90.779	90.787
γ (deg)	90	90
V ($Å^3$)	699.74(3)	699.84(3)
Z	4	4
Dc (g/cm^3)	1.577	1.577
μ (mm^{-1})	0.129	0.129
F (000)	344	344
h_{max}, k_{max}, l_{max}	5, 22, 15	5, 22, 15
$Theta_{max}$	28.8270	29.207
CCDC	2127284	2127281

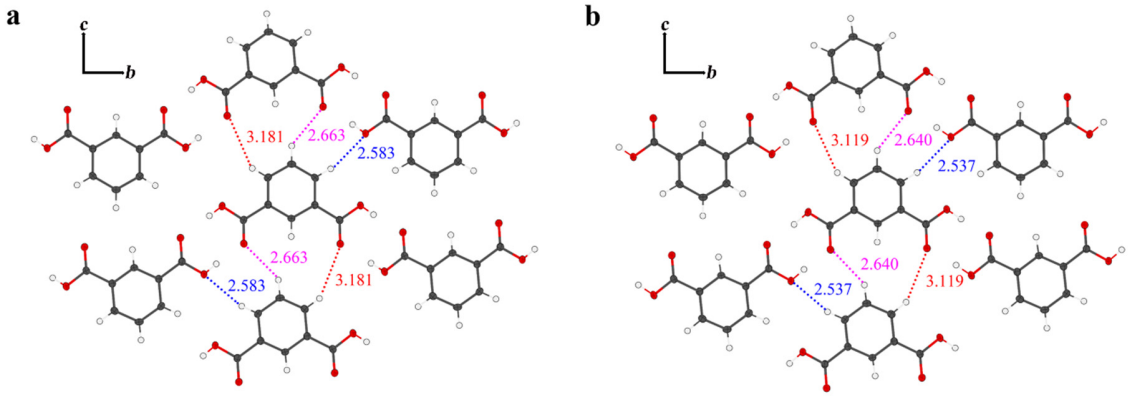

Fig. S60. (a) The intermolecular interactions and distances between adjacent IPA molecules before irradiation (*a*-axis, from single crystal). (b) The intermolecular interactions and distances between adjacent IPA molecules after irradiation (*a*-axis, from single crystal).

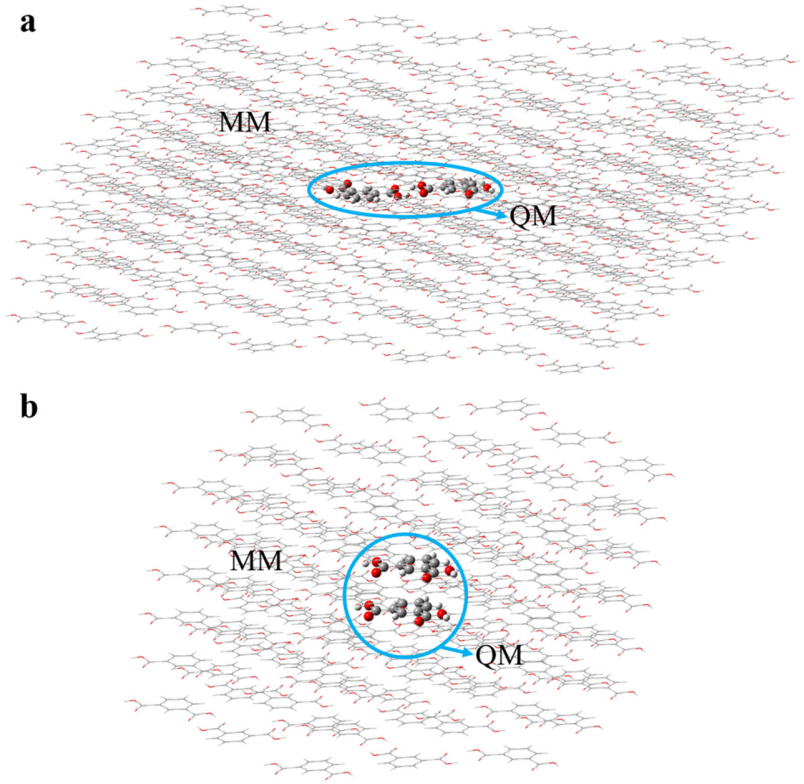

Fig. S61. Two-layer ONIOM model of IPA structure: (a) the hydrogen bond dimer. (b) the π–π molecular stacking dimer.

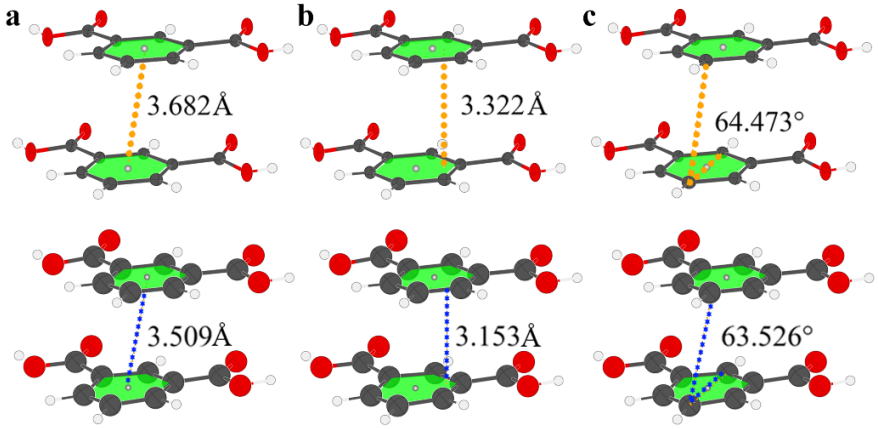

Fig. S62. Molecular packing modes of PA before photo-activation (from single crystal) and after photo-activation (from TD-DFT calculating). (a) Plane centroid to plane centroid distance of IPA before photo-activation (up) and after photo-activation (down). (b) Plane to plane distance of PA before photo-activation (up) and after photo-activation (down). (c) The slip angle between π-stacked molecules of PA before photo-activation (up) and after photo-activation (down), respectively.

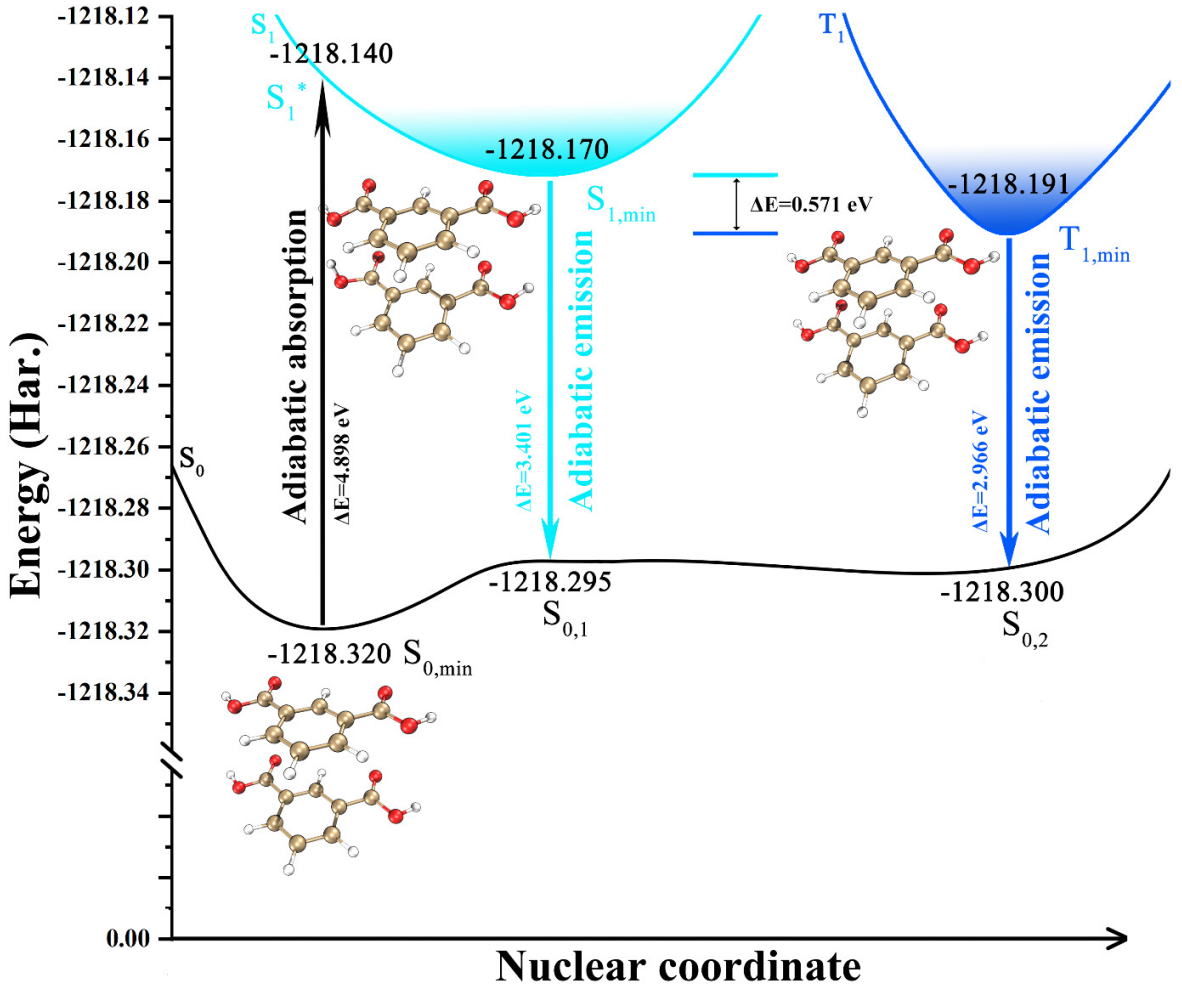

Fig. S63. The energy and the structure of the IPA dimer at S_0, S_1 and T_1 state.

Table S5. Singlet and triplet excited states' energy levels of two IPA dimers from TD-DFT calculated by Gaussian 09, Revision E.01.

Excited state	Hydrogen bond dimer		π–π molecular stacking dimer	
	Energy level(eV) / wavelength(nm)	*f*	Energy level(eV) / wavelength(nm)	*f*
S_1	3.7157 / 333.68	0.0002	3.2356 / 383.19	0.0004
S_2	4.9650 / 249.72	0.0443	4.8499 / 255.64	0.0173
S_3	5.1327 / 241.56	0.0023	4.9546 / 250.24	0.0003
T_1	3.0840 / 402.02	-	2.9664 / 417.96	-
T_2	4.0169 / 308.66	-	3.9123 / 316.91	-
T_3	4.2929 / 288.81	-	4.2605 / 291.01	-
T_4	4.4622 / 277.85	-	4.3043 / 288.05	-
T_5	4.7856 / 259.08	-	4.4178 / 280.65	-
T_6	4.7940 / 258.62	-	4.6499 / 266.64	-
T_7	4.8040 / 258.09	-	4.6778 / 265.05	-
T_8	4.8126 / 257.63	-	4.6810 / 264.87	-
T_9	4.8801 / 254.06	-	4.6879 / 264.48	-
T_{10}	5.0987 / 243.17	-	4.7067 / 263.42	-

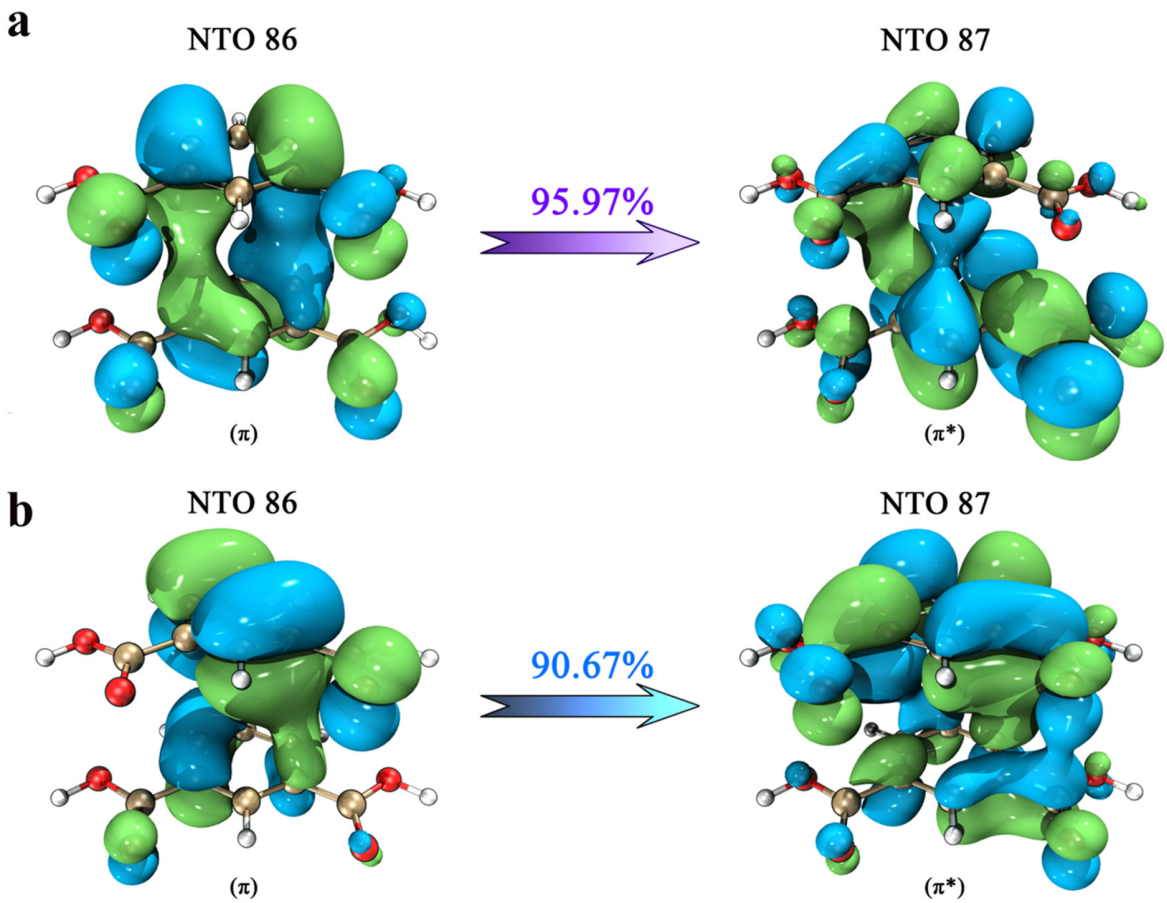

Fig. S64. Natural transition orbitals (NTOs) of π–π molecular stacking dimer for (a) S_1 and (b) T_1 and their π-π*/ π-π*characteristic.

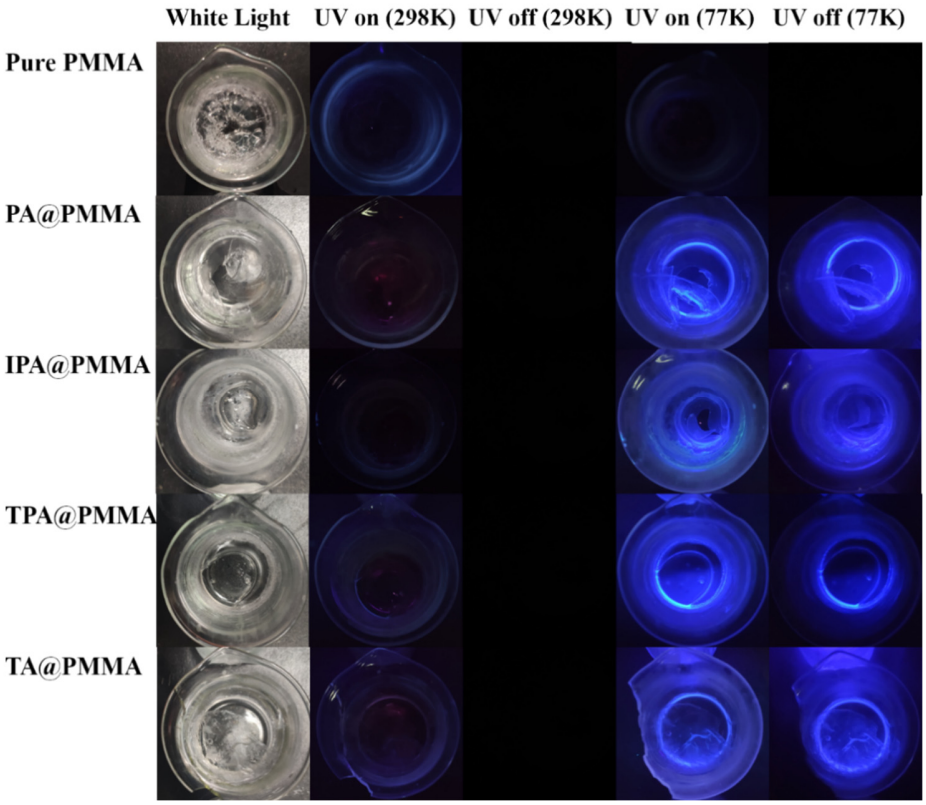

Fig. S65. The photo of BADs@PMMA under white light and 254 nm handy UV lamp in 298 K and 77 K conditions.

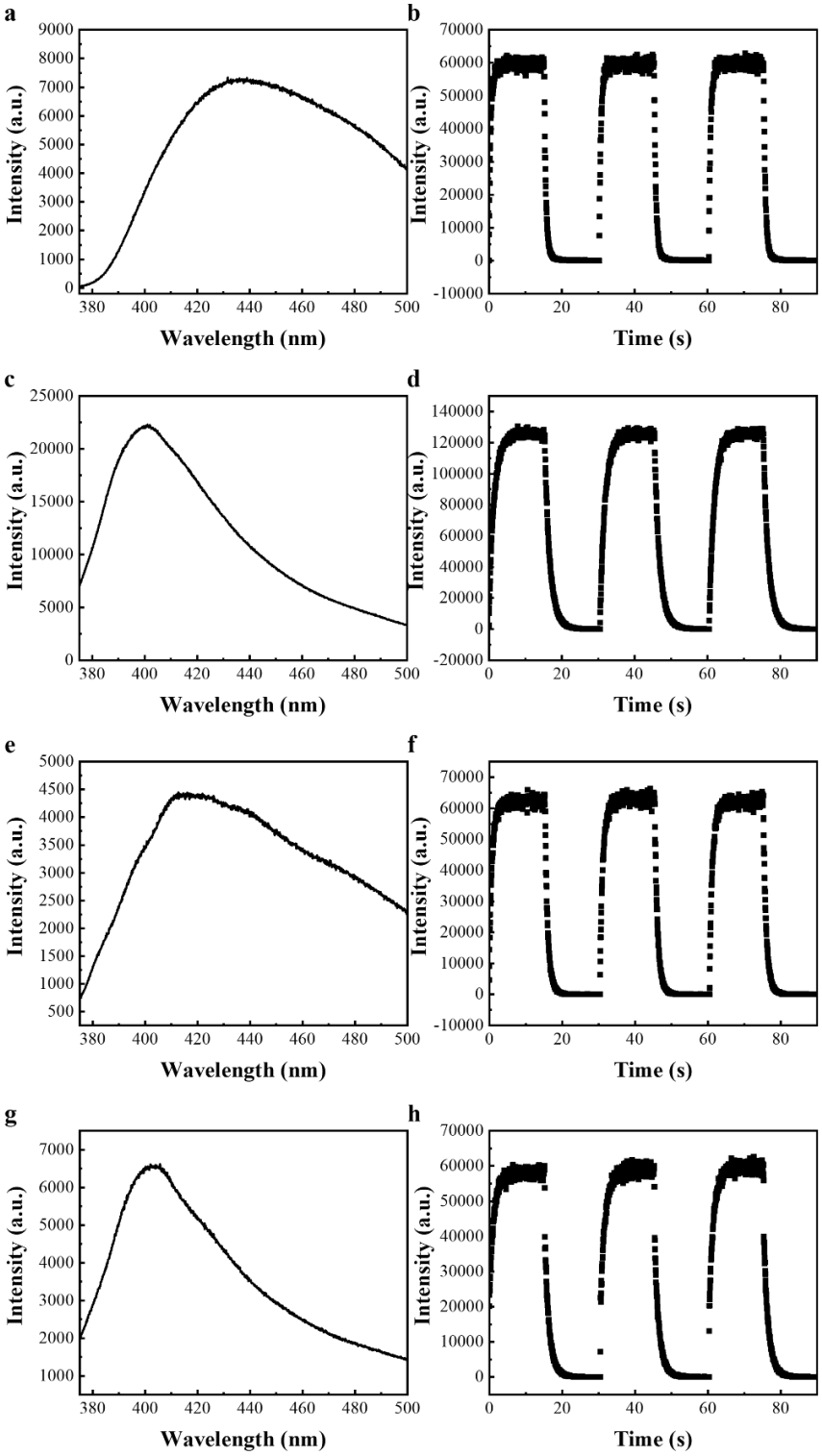

Fig. S66. (a) and (b) the phosphorescence spectrum and photo-activation cycles of PA@BA. (c) and (d) the phosphorescence spectrum and photo-activation cycles of IPA@BA. (e) and (f) the

phosphorescence spectrum and photo-activation cycles of TPA@BA. (g) and (h) the phosphorescence spectrum and photo-activation cycles of TA@BA.

References

1. M. J. Frisch, G. W. Trucks, H. B. Schlegel, G. E. Scuseria, M. A. Robb, J. R. Cheeseman, G. Scalmani, V. Barone, B. Mennucci, G. A. Petersson, H. Nakatsuji, M. Caricato, X. Li, H. P. Hratchian, A. F. Izmaylov, J. Bloino, G. Zheng, J. L. Sonnenberg, M. Hada, M. Ehara, K. Toyota, R. Fukuda, J. Hasegawa, M. Ishida, T. Nakajima, Y. Honda, O. Kitao, H. Nakai, T. Vreven, J. A. Montgomery, Jr., J. E. Peralta, F. Ogliaro, M. Bearpark, J. J. Heyd, E. Brothers, K. N. Kudin, V. N. Staroverov, T. Keith, R. Kobayashi, J. Normand, K. Raghavachari, A. Rendell, J. C. Burant, S. S. Iyengar, J. Tomasi, M. Cossi, N. Rega, J. M. Millam, M. Klene, J. E. Knox, J. B. Cross, V. Bakken, C. Adamo, J. Jaramillo, R. Gomperts, R. E. Stratmann, O. Yazyev, A. J. Austin, R. Cammi, C. Pomelli, J. W. Ochterski, R. L. Martin, K. Morokuma, V. G. Zakrzewski, G. A. Voth, P. Salvador, J. J. Dannenberg, S. Dapprich, A. D. Daniels, O. Farkas, J. B. Foresman, J. V. Ortiz, J. Cioslowski, and D. J. Fox, Gaussian 09, Revision E.01; Gaussian, Inc., Wallingford, CT, 2013.

2. Y. Zhao and D. G. Truhlar, *Theor. Chem. Acc.,* 2007, **120**, 215-241.

3. L. W. Chung, W. M. Sameera, R. Ramozzi, A. J. Page, M. Hatanaka, G. P. Petrova, T. V. Harris, X. Li, Z. Ke, F. Liu, H. Bei, L. Ding and K. Morokuma, *Chem. Rev.,* 2015, **115**, 5678-5796.

4. O. V. Dolomanov, L. J. Bourhis, R. J. Gildea, J. A. K. Howard and H. Puschmann, *J. Appl. Cryst.,* 2009, **42**, 339-341.

5. T. Lu and F. Chen, *J. Comput. Chem.,* 2012, **33**, 580-592.

6. W. Humphrey, A. Dalke and K. Schulten, *J. Molec. Graphics,* 1996, **14**, 33-38.